Comptonellins A–H, Highly Potent Antiviral Ternatin-type Cyclopeptides from Comptonella drupacea

Cécile Apel, Juliano Haddad, Charline Herrscher, Clément Grisel, Justine Girard, Florent Olivon, Cyril Poullain, Jean-François Gallard, Stéphanie Boutet, Fanny Roussi, et al.

Comptonellins A-H, Highly Potent Antiviral Ternatin-type Cyclopeptides from *Comptonella drupacea*

Cécile Apel,[1,*] Juliano Haddad,[2] Charline Herrscher,[2] Clément Grisel,[1] Justine Girard,[2] Florent Olivon,[1] Cyril Poullain,[3] Jean-François Gallard,[1] Stéphanie Boutet,[4] Fanny Roussi,[1] Sandy Desrat,[1] Chaker El Kalamouni[2,*] and Marc Litaudon[1,*]

[1] Université Paris-Saclay, CNRS, Institut de Chimie des Substances Naturelles, UPR 2301, 91198, Gif-sur-Yvette, France

[2] Unité Mixte Processus Infectieux en Milieu Insulaire Tropical, Université de la Réunion, INSERM U1187, CNRS UMR 9192, IRD UMR 249, Plateforme Technologique CYROI, 94791 Sainte Clotilde, France

[3] Laboratoire de Chimie Bio-inspirée et d'Innovations Ecologiques, ChimEco, UMR 5021 CNRS – UM, Cap Delta, 1682 Rue de la Valsière, 34790 Grabels, France

[4] Institut Jean-Pierre Bourgin (IJPB), AgroParisTech, INRAE, Université Paris-Saclay, 78000, Versailles, France

Corresponding authors:

*CA, Tel: +33 1 69 82 30 38. E-mail: cecile.apel@cnrs.fr

*CEK, Tel: +262 262 93 91 95. E-mail: chaker.el-kalamouni@univ-reunion.fr

*ML, Tel: +33 1 69 82 30 38. E-mail: marc.litaudon@cnrs.fr

ABSTRACT

An antiviral screening of plant extracts from Rutaceae and Annonaceae families led to the isolation of a series of new cycloheptapeptides, comptonellins A-H (**1**-**8**), along with the known ternatin (**9**). These compounds were isolated from the ethyl acetate bark extract of *Comptonella drupacea* (Labill.) Guillaumin, an endemic Rutaceae species of New Caledonia. Following targeted isolation guided by multi-informative molecular networks, the structures of compounds **1**-**9** were elucidated through a comprehensive analysis of spectroscopic data. This revealed novel molecules featuring previously unreported and non-canonical amino acids. The absolute configuration of stereocenters was partially determined by advanced Marfey's method. Biological evaluation against Zika virus demonstrated the potent antiviral properties of comptonellin A and comptonellins C-G, with IC_{50} values ranging from 7 to 240 nM. Further investigations revealed that comptonellin A displayed broad-spectrum antiviral activity, inhibiting Dengue virus, Ross River virus and SARS-CoV-2. These findings highlight comptonellins as promising antiviral scaffolds, supporting further investigation into their therapeutic potential against emerging viral infections.

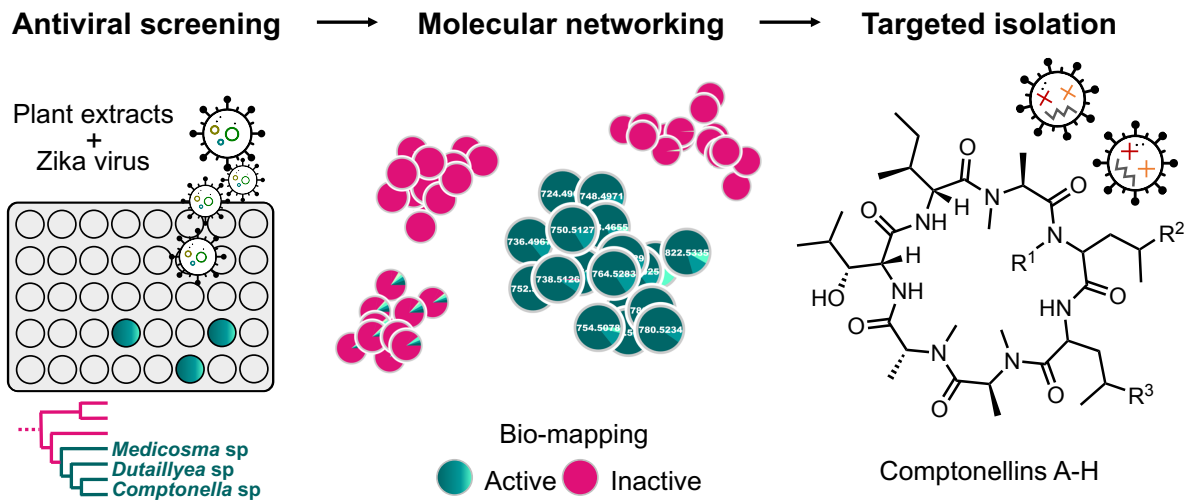

INTRODUCTION

Arboviruses, including Zika (ZIKV), dengue (DENV), West Nile (WNV), yellow fever (YFV), and chikungunya (CHIKV) viruses, represent a major public health threat, with millions of cases reported annually due to their rapid geographical expansion and the increasing burden of associated diseases.[1] These viruses, primarily transmitted by *Aedes* mosquitoes, have caused numerous epidemics worldwide, exacerbated by climate change, urbanization, trade and global travel.[2–8] Despite the availability of vaccines for certain arboviruses, effective antiviral treatments remain scarce and current management strategies rely predominantly on vector control and supportive care.[9–12] The lack of broad-spectrum antiviral therapies underscores the need to explore novel molecular targets for antiviral drug development.

One of the key challenges in combating these viruses lies in their ability to hijack host cellular processes to facilitate their replication. Unlike direct-acting antivirals that target viral components, an alternative and potentially broader-spectrum strategy is to develop host-directed therapies that interfere with cellular factors essential for viral replication.[13] Such approaches may offer cross-protection against multiple arboviruses, thereby addressing the limitations of viral genetic variability and drug resistance.[14]

With the aim of identifying new natural bioactive compounds, we have recently described a set of 824 plant extracts from the ICSN (Institut de Chimie des Substances Naturelles, France) extract library, derived from Rutaceae and Annonaceae species collected in New Caledonia, Vietnam and Malaysia.[15,16] These botanical families were selected based on the large number of specimens available in our collection and the high degree of endemism among the species included. These criteria are expected to provide access to a broader, possibly novel and unexplored chemical space. We have also proposed an approach employing molecular

networking enriched with bioactivity and taxonomy information, to identify potentially original bioactive molecules within crude extract collections.[17–20]

In the present study, we applied our methodology to the same set of 824 extracts, intending to discover compounds with antiviral properties, particularly against ZIKV, as an orthoflavivirus model. Through a phenotypic cell-based assay, we uncovered several extracts displaying anti-ZIKV activity, in particular the ethyl acetate (EtOAc) bark extract of the Rutaceae *Comptonella drupacea* (Labill.) Guillaumin. This species is a small to medium-sized tree, reaching up to twelve meters high and is found in dense humid forests and maquis of New Caledonia. The genus is endemic and comprises eight species according to the last revision of Hartley, *C. baudouinii*, *C. drupacea*, *C. fruticosa*, *C. glabra*, *C. lactea*, *C. microcarpa*, *C. oreophila* and *C. sessilifoliola*.[21] A few previous phytochemical studies have described the presence of alkaloids and flavonoids in this genus.[22–25]

Here we report the targeted isolation and antiviral activity of the known cyclopeptide ternatin (**9**) and eight previously undescribed related analogues, comptonellins A-H (**1**-**8**), from the bark of *C. drupacea*.

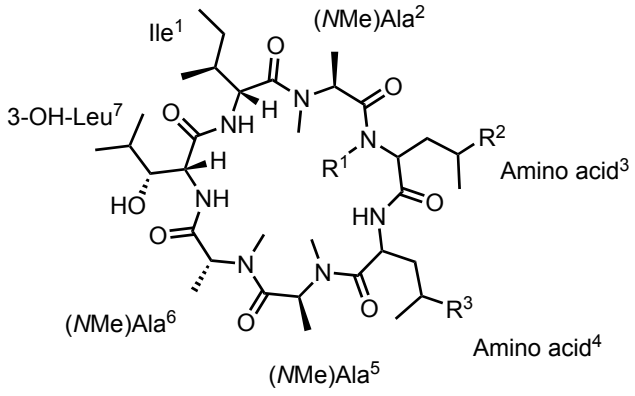

1: $R^1 = CH_3$; $R^2 = CH_3$; $R^3 = CHCH_2$
2: $R^1 = H$; $R^2 = CH_3$; $R^3 = CHCH_2$
3: $R^1 = CH_3$; $R^2 = CH_2CH_3$; $R^3 = CHCH_2$
4: $R^1 = CH_3$; $R^2 = CH_2OH$; $R^3 = CHCH_2$
5: $R^1 = CH_3$; $R^2 = CHOHCH_3$; $R^3 = CHCH_2$
6: $R^1 = CH_3$; $R^2 = CH_2OCHO$; $R^3 = CHCH_2$
7: $R^1 = CH_3$; $R^2 = CH(OCHO)CH_3$; $R^3 = CHCH_2$
8: $R^1 = CH_3$; $R^2 = CH_2OH$; $R^3 = CH_3$
9: $R^1 = CH_3$; $R^2 = CH_3$; $R^3 = CH_3$

RESULTS AND DISCUSSION

Screening of Rutaceae and Annonaceae Extracts for Antiviral Activity against Zika Virus. A collection of 38 alkaloid extracts and 786 polyamide-filtered EtOAc extracts was set up from different parts of 86 Rutaceae and 135 Annonaceae species. The extract library was screened using human lung A549 cells infected with an infectious molecular clone of ZIKV harboring a Green Fluorescent Protein reporter gene ($ZIKV^{GFP}$), resulting in GFP expression in infected cells.[26] The initial screening, performed at 200 µg/mL, identified several extracts that inhibited viral infection by more than 90%, compared to untreated infected cells. The most active extracts were subsequently evaluated in a dose-response assay, which led to the identification of eight extracts, all from New Caledonian Rutaceae species, with half maximal inhibitory concentration (IC_{50}) values ranging from 0.52 to 8.79 µg/mL and moderate cytotoxicity, with CC_{50} values above 100 µg/mL, suggesting a favorable selectivity profile. Interestingly, within the Rutaceae collection from New Caledonia, which encompasses 17 genera, the eight active extracts originated from phylogenetically close taxa, namely *Comptonella* and *Dutaillyea*, belonging to the clade 1 of the *Acronychia-Melicope* clade, as well as *Medicosma*, sister to the same clade.[27]

Molecular Networking-Guided Isolation of Bioactive Compounds. To further investigate the chemical diversity associated with antiviral activity, the entire collection of Rutaceae extracts, comprising 332 samples, was analyzed by LC-$HRMS^2$ in data-dependent acquisition mode. The spectral data were processed with MZmine 4[28] and organized as molecular networks using MetGem.[29] The antiviral activity data were classified into five levels (<5, 5-10, 10-50, 50-100 and >100 µg/mL) based on the IC_{50} values of the extracts. Integrating these data into the networks enabled the differentiation of ions detected in active extracts (shades of green)

from those present in inactive extracts (pink) (**Figure 1**). This revealed three distinct clusters specific to the active extracts (**Figure 1A)**, corresponding to groups of $[M+H]^+$, $[M+NH_4]^+$ and $[M+Na]^+$ adducts of the same structural analogues. Furthermore, the taxonomic mapping of the botanical genera showed that this family of compounds was very specific to the clade mentioned above (**Figure 1B**), reinforcing the hypothesis that this group of molecules could be responsible for the antiviral activity observed in the eight active Rutaceae extracts. The attempt to annotate those compounds of interest by searching for standards and analogues in GNPS spectral libraries (https://gnps.ucsd.edu/ProteoSAFe/libraries.jsp) did not yield any matches. However, molecular formula, fingerprint and class prediction by Sirius[30] suggested cycloheptapeptide-type compounds. Therefore, the targeted isolation of these molecules, which likely have active, original and/or undescribed structures was undertaken. The bark extract of *C. drupacea* was chosen among the eight active extracts because of its most interesting activity value (IC_{50} 0.52 µg/mL), and because it presented a greater diversity of cyclopeptide analogues.

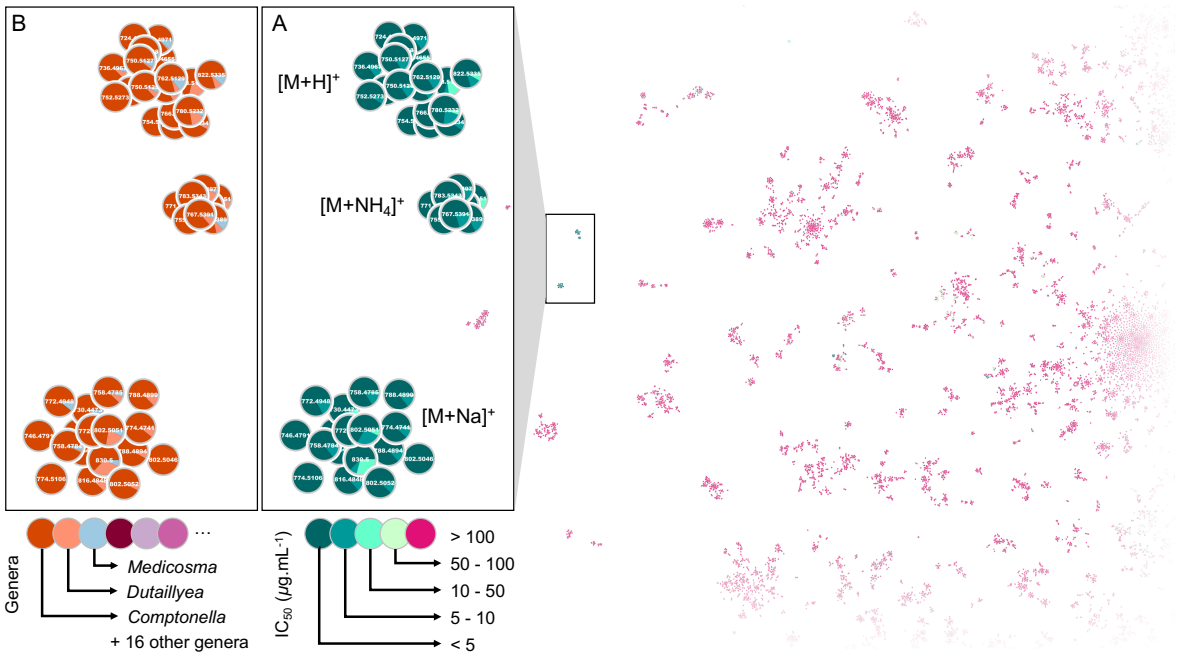

Figure 1. Molecular networks generated from 332 LC-MS[2] analyses of Rutaceae extracts. The bioactivity mapping highlights three clusters of ions specific to active extracts (**A**). The

taxonomic mapping shows the exclusive production of the corresponding compounds by the closely related genera *Comptonella*, *Dutaillyea* and *Medicosma* (**B**).

Structure Elucidation of Compounds Isolated from *C. drupacea*. After extraction and purification, compound **1** was obtained as a yellow amorphous solid. Its HRESIMS data showed a $[M + H]^+$ ion peak at *m/z* 750.5121 (calcd for $C_{38}H_{68}N_7O_8^+$ 750.5124) and a sodium adduct $[M + Na]^+$ at *m/z* 772.4938 (calcd for $C_{38}H_{67}N_7O_8Na^+$ 772.4943) corresponding to the molecular formula $C_{38}H_{67}N_7O_8$ and indicating nine degrees of unsaturation (**Figure S1**). The ^{1}H NMR spectrum of **1** in CD_3CN showed three amide NH doublets at δ_H 7.48, 7.39, 6.99, seven α-amino proton signals in the region of δ_H 4.02-5.45, three olefinic protons (δ_H 4.93, 5.02, 5.69), four *N*-methyl singlets (δ_H 2.86, 2.94, 2.96, 3.05) and ten methyl signals (δ_H 0.86-1.26) (**Figure S2, Table 1**). The ^{13}C NMR spectrum contained seven amide-type carbonyl signals (δ_C 169.5-175.9), two vinylic carbons (δ_C 115.7, 143.6) and an oxygenated methine (δ_C 76.8) (**Figure S3, Table 1**). The investigation of COSY, TOCSY, HSQC-TOCSY, HSQC, HMBC and ROESY spectra allowed the identification of seven amino acids, one isoleucine (Ile), one *N*-methyl leucine [(*N*Me)Leu], one hydroxyleucine (3-OH-Leu), three *N*-methyl alanines [(*N*Me)Ala] and the unusual 2-amino-4-methyl-5-hexenoic acid (dehydromethyl-leucine, dhML) residue. The TOCSY correlations from the methylene protons H-εa and H-εb to H-δ, H-γ, H$_3$-δ', H-βa, H-βb and H-α, as well as the COSY correlation from H-α to NH highlighted the spin system of the dhML[4] fragment. The HMBC correlations from H-α to C-γ, H-βa and H-βb to C-δ, H$_3$-δ' to C-β and C-δ and from H-εa to C-γ confirmed the structure of the residue (See TOCSY and HMBC correlations **Figure 2** and spectra **Figures S4-S9**). All features accounted for eight of nine degrees of unsaturation, suggesting the cyclic structure of **1**.

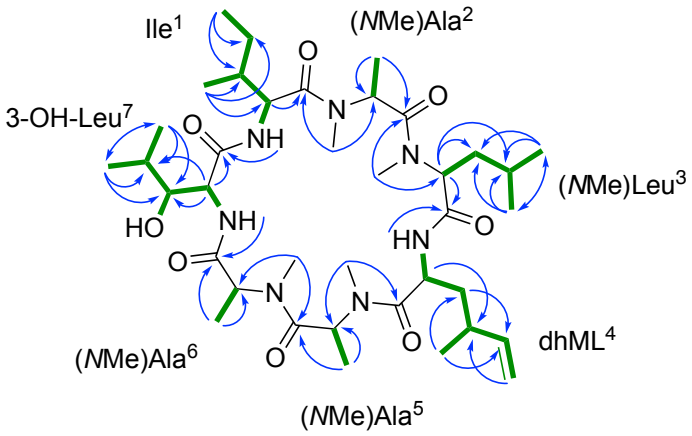

Figure 2. TOCSY (bold) and HMBC (arrows) correlations of **1**.

The sequence of the amino acid residues was defined using HMBC correlations observed from each NH or *N*Me to its respective adjacent carbonyl. The correlations from Ile[1]-NH to 3-OH-Leu[7]-CO, 3-OH-Leu[7]-NH to (*N*Me)Ala[6]-CO, (*N*Me)Ala[6]-*N*Me to (*N*Me)Ala[5]-CO, (*N*Me)Ala[5]-*N*Me to dhML[4]-CO, dhML[4]-NH to (*N*Me)Leu[3]-CO, (*N*Me)Leu[3]-*N*Me to (*N*Me)Ala[2]-CO and (*N*Me)Ala[2]-*N*Me to Ile[1]-CO, indicated that **1** was linked in a cyclo-sequence [Ile[1], (*N*Me)Ala[2], (*N*Me)Leu[3], dhML[4], (*N*Me)Ala[5], (*N*Me)Ala[6], 3-OH-Leu[7]]. Analysis of ESI-MS/MS fragmentation patterns in the positive mode indicated that cleavages occur predominantly at the C-terminal of *N*Me-Ala[2,5,6], as evidenced by the key MS/MS fragments at *m/z* 423 and 338, followed by the sequential losses of *N*Me-Ala[5] and dhML[4] (*m/z* 253 and 128) (**Figures S10-11**). Furthermore, the peaks at *m/z* 625, 498, 413, 300, 171 and 86 demonstrated the sequential cleavage of dhML[4], (*N*Me)Leu[3], (*N*Me)Ala[2], Ile[1], 3-OH-Leu[7], (*N*Me)Ala[6] and (*N*Me)Ala[5] and confirmed the sequence of the heptapeptide. The structure of compound **1** was closely related to the natural peptide ternatin,[31] which was also isolated in the present study (See HRESIMS and NMR data of ternatin (**9**) **Figures S12-20**). The difference was the presence of dhML[4] in **1** instead of Leu in ternatin (**9**). The absolute configurations of the amino acid residues of **1** were partially assigned by UHPLC-MS analysis of its acid hydrolysate derivatized with Marfey's reagent (1-fluoro-2,4-dinitrophenyl-5-L-alanine amide). Two L-(*N*Me)Ala, one D-(*N*Me)Ala

and L-(*N*Me)Leu were identified by comparison with retention times of commercially available standards (**Figure S21**). The stereochemistry of Ile[1] was determined to be either D- or D-*allo*, and that of 3-OH-Leu[7] as either L or D. The NH proton signals of 3-OH-Leu[7] and dhML[4] remained visible in the ^{1}H NMR spectrum after addition of a small amount of D_2O, suggesting the presence of two intramolecular hydrogen bonds, likely contributing to a rigid conformation for compound **1**. A similar conformational locking has been reported for ternatin, with an additional hydrogen bond involving the hydroxyl group of 3-OH-Leu[7].[31] Although this third hydrogen bond could not be confirmed for **1**, the observed coupling constant of 9.5 *Hz* between the H-α and H-β protons of 3-OH-Leu[7] indicates a trans arrangement, consistent with the structure of ternatin. Assuming a comparable hydrogen bonding network is present, this coupling may reflect a fixed conformation that supports stereochemical assignment. The specific rotation value ($[\alpha]_D^{20}$-33, *c* 0.4, EtOH) of **1** was also similar to that of ternatin. Based on ROESY correlations and comparison with the reported data for ternatin, a plausible absolute configuration for compound **1** is D-*allo*-Ile[1], L-(*N*Me)Ala[2], L-(*N*Me)Leu[3], L-(*N*Me)Ala[5], D-(*N*Me)Ala[6] and β-OH-D-Leu[7] (**Figure S22**).

Only three natural products containing the dhML residue have previously been described.[32] These are also ternatin-type cyclopeptides, for which the synthesis of one of the analogues enabled the (2*S*,4*R*)-stereochemistry of dhML to be determined.[33] We suppose that dhML[4] in **1** has the same stereochemistry, although chemical synthesis must be conducted to assign unambiguously the two stereocenters.

The molecular formula of compound **2** was established as $C_{37}H_{65}N_7O_8$ by HRESIMS, which showed a $[M + H]^+$ ion peak at *m/z* 736.4971 (calcd for $C_{37}H_{66}N_7O_8^+$ 736.4967) (**Figure S23**). NMR spectroscopic data showed similar structural features to those of **1** (**Table 1**, **Figures S25-31**). However, **2** was found to possess a Leu[3] instead of a (*N*Me)Leu[3] as in **1**. This was supported by an additional NH doublet at δ_H 7.16 and one less *N*-methyl singlet in the ^{1}H spectrum. The

TOCSY correlations from Leu^3-NH to H-α, H-βa, H-βb, H-γ, H-δ and H-δ' revealed the complete spin system of Leu^3. The HMBC correlations from Leu^3-NH (δ_H 7.16) to (*N*Me)Ala^2-CO (δ_C 171.3) and from dhML^4-NH (δ_H 7.00) to Leu^3-CO (δ_C 172.3) confirmed the position of the residue (See TOCSY and HMBC correlations **Figure S32**). The presence of this NH in place of an *N*Me considerably affects the chemical shifts of atoms throughout the molecule. This effect probably results from a significant conformational difference between **1** and **2**.

Compound **3** gave the molecular formula $C_{39}H_{69}N_7O_8$, as indicated by HRESIMS of the $[M + H]^+$ ion peak at *m/z* 764.5279 (calcd for $C_{39}H_{70}N_7O_8^+$ 764.5280) (**Figure S33**). The formula suggested the presence of an additional methylene in the structure compared to that of **1**. Its NMR spectra also displayed very similar proton and carbon resonances and cross-correlations with those of **1 (Table 1**, **Figures S34-41)**. The minor structural difference was the presence of (*N*Me)HomoIle^3 in **3** instead of (*N*Me)Leu^3 as in **1**. This was evidenced by the vicinal coupling between the methine hydrogen H-α (δ_H 4.05) and the methylene H_2-β (δ_H 1.07, 2.13), between H-γ (δ_H 1.08) and the methyl H_3-δ (δ_H 0.93) and between H_3-ε (δ_H 0.82) and H_2-δ (δ_H 1.15, 1.29), as well as HMBC correlations from H-α to C-β and C-γ and from H_3-ε to C-δ' and C-γ (See TOCSY and HMBC correlations **Figure S32**).

Compound **4** contains an additional oxygen atom in comparison with compound **1**, as evidenced by its molecular formula $C_{38}H_{67}N_7O_9$ indicated by HRESIMS of the $[M + H]^+$ ion peak at *m/z* 766.5106 (calcd for $C_{38}H_{68}N_7O_9^+$ 766.5073) (**Figure S42**). The NMR spectroscopic data of **4** were very comparable to those of **1** and **3**, but revealed deshielded signals at δ_H 3.25 (H_2-δ) and δ_C 67.8 (C-δ) suggesting the presence of an oxygenated methylene on the (*N*Me)-5-OH-Leu^3 amino acid residue. The vicinal couplings observed from the COSY spectrum together with key HMBC correlations confirmed the structure of the side chain (**Table 2**, **Figures S32, S43-50**).

The structure of compound **5**, which has the formula $C_{39}H_{69}N_7O_9$ (**Figure S51**), only differed from **4** by the possession of an additional methyl group and an oxygenated methine resonating

at δ_H 3.50 (H-δ) and δ_C 71.4 (C-δ) in place of the methylene-δ as in **4** (**Table 2**, **Figures S52-59**). This was deduced from the COSY correlation between the methyl H_3-ε (δ_H 1.00) and the methine δ_H 3.50 (H-δ) and from correlations from H_3-ε to H-δ (δ_H 3.50), H-γ (δ_H 1.17), H-δ' (δ_H 0.92) (TOCSY spectrum) and from H_3-ε to C-δ and C-γ (HMBC spectrum) (**Figure S32**).

HRESIMS data of compound **6** showed a $[M + H]^+$ ion peak at *m/z* 794.5013 (calcd for $C_{39}H_{68}N_7O_{10}^+$ 794.5022) corresponding to the molecular formula $C_{39}H_{67}N_7O_{10}$ and indicating ten degrees of unsaturation (**Figure S60**). The molecule contains an additional unsaturation compared to compounds **1-5**, due to the presence of a formate group at the end of the (*N*Me)-5-formate-Leu^3 side chain. This was supported by the presence of the deshielded signals at δ_H 8.03 (H-ε) and δ_C 162.4 (C-ε) and key correlations observed from 2D NMR spectra: the proton H-ε of the formate group gave an HMBC correlation with the methylene carbon C-δ, a COSY correlation with the methylene proton H-δ and TOCSY correlations with H-δ, H-γ and the methyl-δ' (**Table 2**, **Figures S32, S61-68**). The presence of this formate group in place of a hydroxy group in **4** is the only structural difference between **4** and **6**.

HRESIMS and NMR data analysis of compound **7** ($[M + H]^+$ ion peak at *m/z* 808.5212, calcd for $C_{40}H_{70}N_7O_{10}^+$ 808.5179) suggested the same single structural difference between **5** and **7** as between **4** and **6 (Table 3**, **Figures S32, S69-77)**: the (*N*Me)-5-formate-HomoIle^3 side chain also bears a formate group instead of a hydroxyl group as in **5**.

The molecular formula of compound **8** was established as $C_{37}H_{67}N_7O_9$ by HRESIMS, which showed a $[M + H]^+$ ion peak at *m/z* 754.5084 (calcd for $C_{37}H_{68}N_7O_9^+$ 754.5073) (**Figure S78**). Its NMR data suggested very similar structural features to **4**, comprising a (*N*Me)-5-OH-Leu^3 amino acid residue, but with dhML^4 replaced by a Leu^4 residue as in ternatin (**9**) (**Table 3**, **Figures S32, S79-86**).

Table 1. ^{1}H NMR (700 MHz) and ^{13}C NMR (175 MHz) data of **1-3** in CD_3CN.

1			2			3		
position	δ_C, type	δ_H, mult. (J in Hz)	position	δ_C, type	δ_H, mult. (J in Hz)	position	δ_C, type	δ_H, mult. (J in Hz)
Ile[1]			**Ile[1]**			**Ile[1]**		
NH		6.99, d (5.8)	NH		7.06, d (5.8)	NH		7.01, d (5.8)
CO	173.7, C		CO	175.7, C		CO	173.7, C	
α	56.2, CH	4.65, dd (5.8, 3.5)	α	56.9, CH	4.44, dd (7.9, 5.8)	α	56.2, CH	4.65, dd (5.8, 3.5)
β	34.6, CH	1.85, m	β	36.9, CH	1.77[a], m	β	34.6, CH	1.85, m
γa	27.3, CH_2	1.40, m	γa	26.1, CH_2	1.18, m	γa	27.3, CH_2	1.40, m
γb		1.50, m	γb		1.44, m	γb		1.50, m
γ ’	14.1, CH_3	0.91, d (7.0)	γ ’	15.7, CH_3	1.02, d (7.0)	γ ’	14.1, CH_3	0.91, d (7.0)
δ	12.1, CH_3	0.94, t (7.5)	δ	12.0, CH_3	0.91, t (7.5)	δ	12.1, CH_3	0.94[a], m
(*N*Me)Ala[2]			**(*N*Me)Ala[2]**			**(*N*Me)Ala[2]**		
N-Me	30.5, CH_3	2.96, s	N-Me	31.7, CH_3	3.08, s	N-Me	30.5, CH_3	2.97, s
CO	170.0, C		CO	171.3, C		CO	170.0, C	
α	50.7, CH	5.45, q (6.5)	α	52.3, CH	5.15, q (7.0)	α	50.7, CH	5.46, q (6.5)
β	15.8, CH_3	1.15, d (6.5)	β	13.1, CH_3	1.21, d (7.0)	β	15.8, CH_3	1.16, d (6.5)
(*N*Me)Leu[3]			**Leu[3]**			**(*N*Me)HomoIle[3]**		
N-Me	29.9, CH_3	2.86, s	NH		7.16, d (7.2)	N-Me	29.9, CH_3	2.87, s
CO	169.6, C		CO	172.3, C		CO	169.5, C	
α	59.7, CH	4.02, dd (11.2, 3.9)	α	54.2, CH	3.55, m	α	59.5, CH	4.05, dd (11.2, 3.9)
βa	40.2, CH_2	1.15[a], m	βa	37.1, CH_2	1.71, m	βa	38.2, CH_2	1.07, m
βb		2.05, m	βb		1.89, m	βb		2.13, m
γ	25.9, CH	1.35, m	γ	25.7, CH	1.55, m	γ	31.8, CH	1.08, m
δ	23.9, CH_3	0.86, d (6.7)	δ	23.7, CH_3	0.88, d (6.7)	δa	31.2, CH_2	1.15[a], m
δ ’	22.8, CH_3	0.93, d (6.7)	δ ’	21.5, CH_3	0.83, d (6.7)	δb		1.29, m
						δ ’	19.6, CH_3	0.93[a], m
						ε	11.6, CH_3	0.82, t (7.3)
dhML[4]			**dhML[4]**			**dhML[4]**		
NH		7.48, d (8.6)	NH		7.00, d (9.0)	NH		7.49, d (8.6)
CO	174.7, C		CO	176.0, C		CO	174.7, C	
α	50.3, CH	4.74, ddd (12.0, 8.6, 2.0)	α	50.4, CH	4.76[a], m	α	50.3, CH	4.75, ddd (12.0, 8.6, 2.0)
βa	36.7, CH_2	1.69, ddd (14.7, 12.0, 3.2)	βa	36.7, CH_2	1.77[a], m	βa	36.7, CH_2	1.70, ddd (14.7, 12.0, 3.2)
βb		1.54, ddd (14.7, 11.0, 2.0)	βb		1.49, ddd (14.7, 11.5, 1.7)	βb		1.54, ddd (14.7, 11.0, 2.0)
γ	36.8, CH	2.14[a], m	γ	36.1, CH	2.24, m	γ	36.8, CH	2.14[a], m
δ	143.6, CH	5.69, ddd (17.0, 10.0, 8.9)	δ	143.1, CH	5.67, m	δ	143.6, CH	5.69, ddd (17.0, 10.0, 8.9)
δ ’	21.4, CH_3	0.99, d (7.0)	δ ’	21.1, CH_3	0.98, d (6.8)	δ ’	21.4, CH_3	0.99, d (7.0)
εa	115.7, CH_2	4.93, dd (17.0, 1.5)	εa	116.8, CH_2	5.07, brs	εa	115.7, CH_2	4.94, dd (17.0, 1.5)
εb		5.02, dd (10.0, 1.5)	εb		5.09, m	εb		5.02, dd (10.0, 1.5)
(*N*Me)Ala[5]			**(*N*Me)Ala[5]**			**(*N*Me)Ala[5]**		
N-Me	31.9, CH_3	3.05, s	N-Me	32.1, CH_3	3.04, s	N-Me	31.9, CH_3	3.06, s
CO	175.9, C		CO	175.8, C		CO	175.9, C	
α	52.4, CH	4.84, q (7.3)	α	52.9, CH	4.77[a], m	α	52.3, CH	4.86, q (7.3)
β	13.7, CH_3	1.33, d (7.3)	β	13.8, CH_3	1.32, d (7.3)	β	13.7, CH_3	1.34, d (7.3)
(*N*Me)Ala[6]			**(*N*Me)Ala[6]**			**(*N*Me)Ala[6]**		
N-Me	31.2, CH_3	2.94, s	N-Me	31.0, CH_3	2.91, s	N-Me	31.2, CH_3	2.95, s
CO	170.5, C		CO	170.3, C		CO	170.5, C	
α	52.6, CH	5.21, q (7.2)	α	52.4, CH	5.22, q (7.2)	α	52.6, CH	5.22, q (7.2)
β	14.3, CH_3	1.26, d (7.2)	β	13.8, CH_3	1.24, d (7.2)	β	14.3, CH_3	1.27, d (7.2)
3-OH-Leu[7]			**3-OH-Leu[7]**			**3-OH-Leu[7]**		
NH		7.39, d (9.5)	NH		7.43, d (9.5)	NH		7.39, d (9.5)
CO	174.3, C		CO	172.8, C		CO	174.3, C	
α	55.9, CH	4.70, t (9.5)	α	55.4, CH	4.70, dd (9.5, 5.5)	α	55.8, CH	4.71, t (9.5)
β	76.8, CH	3.48, d (9.5)	β	80.1, CH	3.50, t (5.5)	β	76.8, CH	3.47, dd (9.5, 1.5)
β ’-OH		5.15, brs	β ’-OH		4.58, brs	β ’-OH		5.14, brs
γ	29.3, CH	1.78, h (7.0)	γ	30.1, CH	1.98, m	γ	29.3, CH	1.79, m
δ	14.8, CH_3	0.93[a], m	δ	17.3, CH_3	0.92, d (6.6)	δ	14.8, CH_3	0.93[a], m
δ ’	21.2, CH_3	0.98, d (7.0)	δ ’	20.5, CH_3	1.01, d (6.6)	δ ’	21.2, CH_3	0.98, d (7.0)

Adapted from WO2024231530, CNRS, INSERM, Univ. La Réunion, IRD. [a]Overlapped

Table 2. ^{1}H NMR (700 MHz) and ^{13}C NMR (175 MHz) data of **4-6** in CD_3CN.

4			**5**			**6**		
position	δ_C, type	δ_H, mult. (J in Hz)	position	δ_C, type	δ_H, mult. (J in Hz)	position	δ_C, type	δ_H, mult. (J in Hz)
Ile[1]			**Ile[1]**			**Ile[1]**		
NH		7.10, d (5.8)	NH		7.04, d (5.8)	NH		7.05, d (5.8)
CO	173.7, C		CO	173.6, C		CO	173.7, C	
α	56.3, CH	4.65, dd (6.0, 3.5)	α	56.2, CH	4.65, dd (5.8, 3.5)	α	56.3, CH	4.65, dd (6.0, 3.5)
β	34.6, CH	1.86, m	β	34.6, CH	1.86, m	β	34.5, CH	1.86, m
γa	27.3, CH_2	1.40, m	γa	27.3, CH_2	1.40, m	γa	27.3, CH_2	1.41, m
γb		1.50, m	γb		1.50, m	γb		1.51, m
γ '	14.1, CH_3	0.91, d (7.0)	γ '	14.1, CH_3	0.91, d (7.0)	γ '	14.1, CH_3	0.91, d (7.0)
δ	12.1, CH_3	0.93[a],m	δ	12.1, CH_3	0.94[a], m	δ	12.1, CH_3	0.94[a],m
(*N*Me)Ala[2]			**(*N*Me)Ala[2]**			**(*N*Me)Ala[2]**		
N-Me	30.5, CH_3	2.97, s	N-Me	30.5, CH_3	2.97, s	N-Me	30.5, CH_3	2.97, s
CO	170.0, C		CO	170.0, C		CO	170.0, C	
α	50.8, CH	5.46, q (6.5)	α	50.8, CH	5.45, q (6.5)	α	50.7, CH	5.46, q (6.5)
β	15.8, CH_3	1.16, d (6.5)	β	15.8, CH_3	1.16, d (6.5)	β	15.8, CH_3	1.16, d (6.5)
(*N*Me)-5-OH-Leu[3]			**(*N*Me)-5-OH-HomoIle[3]**			**(*N*Me)-5-OH-formyl-Leu[3]**		
N-Me	29.9, CH_3	2.88, s	N-Me	29.9, CH_3	2.88, s	N-Me	29.8, CH_3	2.87, s
CO	169.7, C		CO	169.6, C		CO	169.1, C	
α	59.5, CH	4.08, dd (11.5, 3.7)	α	59.7, CH	4.06, dd (12.0, 3.7)	α	59.1, CH	4.08, dd (11.5, 3.7)
βa	34.7, CH_2	1.07, ddd (13.2, 9.5, 3.7)	βa	34.5, CH_2	1.10, ddd (13.2, 9.5, 3.7)	βa	34.6, CH_2	1.16, m
βb		2.23, ddd (13.2, 11.5, 4.0)	βb		2.25, ddd (13.2, 12.0, 2.8)	βb		2.24, m
γ	33.5, CH	1.32[a], m	γ	37.1, CH	1.17[a], m	γ	30.3, CH	1.56, m
δ	67.8, CH_2	3.25, m	δ	71.4, CH	3.50, dq (6.3, 4.3)	δ	69.3, CH_2	3.90, m
δ '	17.3, CH_3	0.925[a], m	δ '	14.9, CH_3	0.92[a], m	δ '	16.9, CH_3	1.00[a], m
δ-OH			δ-OH			CHO	162.4, CH	8.03, s
			ε	20.1, CH_3	1.00[a], m			
dhML[4]			**dhML[4]**			**dhML[4]**		
NH		7.56, d (8.7)	NH		7.53, d (8.6)	NH		7.53, d (8.7)
CO	174.7, C		CO	174.6, C		CO	174.6, C	
α	50.4, CH	4.75, ddd (12.0, 8.6, 2.0)	α	50.4, CH	4.74, ddd (12.0, 8.6, 2.0)	α	50.4, CH	4.74, m
βa	36.7, CH_2	1.69, ddd (14.7, 12.0, 3.2)	βa	36.6, CH_2	1.69, ddd (14.7, 12.0, 3.2)	βa	36.5, CH_2	1.69, ddd (14.7, 12.0, 3.2)
βb		1.56, ddd (14.7, 11.0, 2.0)	βb		1.55, ddd (14.7, 11.0, 2.0)	βb		1.56, m
γ	36.8, CH	2.14[a], m	γ	36.8, CH	2.14[a], m	γ	36.8, CH	2.14[a], m
δ	143.5, CH	5.70, ddd (17.0, 10.0, 8.9)	δ	143.5, CH	5.69, ddd (17.0, 10.0, 8.9)	δ	143.5, CH	5.69, m
δ '	21.4, CH_3	0.99, d (7.0)	δ '	21.4, CH_3	0.99, d (7.0)	δ '	21.4, CH_3	0.99, d (7.0)
εa	115.8, CH_2	4.94, dd (17.0, 1.5)	εa	115.7, CH_2	4.94, dd (17.0, 1.5)	εa	115.7, CH_2	4.93, dd (17.0, 1.7)
εb		5.02, dd (10.0, 1.5)	εb		5.02, dd (10.0, 1.5)	εb		5.02, dd (10.0, 1.7)
(*N*Me)Ala[5]			**(*N*Me)Ala[5]**			**(*N*Me)Ala[5]**		
N-Me	31.9, CH_3	3.06, s	N-Me	31.9, CH_3	3.06, s	N-Me	31.9, CH_3	3.06, s
CO	175.9, C		CO	175.9, C		CO	175.9, C	
α	52.4, CH	4.86, q (7.3)	α	52.4, CH	4.87, q (7.3)	α	52.3, CH	4.86, q (7.3)
β	13.7, CH_3	1.34, d (7.3)	β	13.7, CH_3	1.34, d (7.3)	β	13.7, CH_3	1.34, d (7.3)
(*N*Me)Ala[6]			**(*N*Me)Ala[6]**			**(*N*Me)Ala[6]**		
N-Me	31.2, CH_3	2.95, s	N-Me	31.2, CH_3	2.95, s	N-Me	31.2, CH_3	2.95, s
CO	170.6, C		CO	170.6, C		CO	170.6, C	
α	52.7, CH	5.22, q (7.2)	α	52.6, CH	5.22, q (7.2)	α	52.7, CH	5.22, q (7.2)
β	14.3, CH_3	1.26, d (7.2)	β	14.3, CH_3	1.27, d (7.2)	β	14.3, CH_3	1.26, d (7.2)
3-OH-Leu[7]			**3-OH-Leu[7]**			**3-OH-Leu[7]**		
NH		7.38, d (9.5)	NH		7.37, d (9.5)	NH		7.37, d (9.5)
CO	174.2, C		CO	174.3, C		CO	174.2, C	
α	55.8, CH	4.72, t (9.5)	α	55.8, CH	4.71, t (9.5)	α	55.8, CH	4.72, t (9.5)
β	76.8, CH	3.48, dd (1.3, 9.5)	β	76.8, CH	3.48, d (9.5)	β	76.8, CH	3.45, d (9.5)
β '-OH		-	β '-OH		5.14, brs	β '-OH		5.16, brs
γ	29.3, CH	1.78, h (7.0)	γ	29.4, CH	1.78, h (7.0)	γ	29.3, CH	1.78, m
δ	14.9, CH_3	0.92[a], m	δ	14.8, CH_3	0.93[a], m	δ	14.9, CH_3	0.93[a], m
δ '	21.2, CH_3	0.98, d (7.0)	δ '	21.3, CH_3	0.98[a], m	δ '	21.2, CH_3	0.98, d (7.0)

Adapted from WO2024231530, CNRS, INSERM, Univ. La Réunion, IRD. [a]Overlapped

Table 3. ^{1}H NMR (700 MHz) and ^{13}C NMR (175 MHz) data of **7-8** in CD_3CN.

7			8		
position	δ_C, type	δ_H, mult. (J in Hz)	position	δ_C, type	δ_H, mult. (J in Hz)
Ile[1]			**Ile[1]**		
NH		7.03, d (5.8)	NH		7.05, d (5.8)
CO	173.7, C		CO	173.6, C	
α	56.3, CH	4.65, dd (5.8, 3.5)	α	56.2, CH	4.64, dd (5.8, 3.5)
β	34.5, CH	1.86, m	β	34.6, CH	1.85, m
γa	27.3, CH_2	1.41, m	γa	27.3, CH_2	1.40, m
γb		1.51, m	γb		1.50, m
γ '	14.1, CH_3	0.91, d (7.0)	γ '	14.1, CH_3	0.91, d (7.0)
δ	12.1, CH_3	0.94[a], m	δ	12.1, CH_3	0.93[a],m
(*N*Me)Ala[2]			**(*N*Me)Ala[2]**		
N-Me	30.5, CH_3	2.97, s	N-Me	30.4, CH_3	2.94, s
CO	170.0, C		CO	170.0, C	
α	50.8, CH	5.45, q (6.5)	α	50.6, CH	5.45, q (6.5)
β	15.8, CH_3	1.16, d (6.5)	β	15.8, CH_3	1.15, d (6.5)
(*N*Me)-5-OH-formyl-HomoIle[3]			**(*N*Me)-5-OH-Leu[3]**		
N-Me	29.8, CH_3	2.87, s	N-Me	29.8, CH_3	2.86, s
CO	169.1, C		CO	169.5, C	
α	59.3, CH	4.06, dd (12.0, 3.7)	α	59.4, CH	4.09, dd (11.5, 3.5)
βa	34.1, CH_2	1.15[a], m	βa	34.8, CH_2	1.07, m
βb		2.23, m	βb		2.23, m
γ	35.0, CH	1.38[a], m	γ	33.5, CH	1.33[a], m
δ	75.1, CH	4.78, quint (6.3)	δ	67.8, CH_2	3.25, m
δ '	15.1, CH_3	0.99[a], m	δ '	17.2, CH_3	0.93[a], m
ε	17.1, CH_3	1.14, d (6.5)	δ-OH		
CHO	162.1, CH	8.02, s			
dhML[4]			**Leu[4]**		
NH		7.52, d (8.6)	NH		7.54, d (8.7)
CO	174.6, C		CO	174.7, C	
α	50.4, CH	4.74, m	α	50.4, CH	4.89, ddd (12.0, 9.5, 2.0)
βa	36.6, CH_2	1.68, m	βa	38.6, CH_2	1.62[a], m
βb		1.55, ddd (14.7, 11.0, 2.0)	βb		1.45, m
γ	36.8, CH	2.14, m	γ	26.3, CH	1.62[a], m
δ	143.5, CH	5.69, m	δ	23.5, CH_3	0.90, d (7.0)
δ '	21.4, CH_3	0.99, d (7.0)	δ '	21.2, CH_3	0.92[a], m
εa	115.7, CH_2	4.94, dd (17.0, 1.5)			
εb		5.02, dd (10.0, 1.5)			
(*N*Me)Ala[5]			**(*N*Me)Ala[5]**		
N-Me	31.9, CH_3	3.06, s	N-Me	32.0, CH_3	3.11, s
CO	175.9, C		CO	175.8, C	
α	52.3, CH	4.87, q (7.3)	α	52.5, CH	4.86, q (7.3)
β	13.7, CH_3	1.34, d (7.3)	β	13.8, CH_3	1.34, d (7.3)
(*N*Me)Ala[6]			**(*N*Me)Ala[6]**		
N-Me	31.2, CH_3	2.95, s	N-Me	31.2, CH_3	2.95, s
CO	170.6, C		CO	170.6, C	
α	52.6, CH	5.22, q (7.2)	α	52.6, CH	5.22, q (7.2)
β	14.3, CH_3	1.27, d (7.2)	β	14.3, CH_3	1.26, d (7.2)
3-OH-Leu[7]			**3-OH-Leu[7]**		
NH		7.35, d (9.5)	NH		7.43, d (9.5)
CO	174.2, C		CO	174.3, C	
α	55.8, CH	4.72, t (9.5)	α	55.9, CH	4.70, t (9.5)
β	76.8, CH	3.45, d (9.5)	β	76.7, CH	3.50, d (9.5)
β '-OH		5.15, brs	β '-OH		
γ	29.3, CH	1.78, h (7.0)	γ	29.3, CH	1.79, m
δ	14.8, CH_3	0.92[a], m	δ	14.8, CH_3	0.92[a], m
δ '	21.3, CH_3	0.99 [a], m	δ '	21.2, CH_3	0.98, d (7.0)

Adapted from WO2024231530, CNRS, INSERM, Univ. La Réunion, IRD. [a]Overlapped

The nine compounds isolated in this study consist of seven amino acids, which differ at positions 3 and 4 of the peptide backbone. Three to four of these amino acids are *N*-methylated, four to five are non-canonical, with three being in the D-configuration, unlike most natural amino acids which are generally in the L-configuration. Due to the commercial unavailability of some of these residues, Marfey's analysis could not be performed and consequently, only part of the stereocenters could be assigned. Some of these amino acids have never been described in the literature, such as those at position 3 of compounds **5**-**7**. However, the question arises as to whether the terminal formate groups in **6** and **7** have an artifactual origin, as they could spontaneously formed by reaction with formic acid used in the mobile phases of liquid chromatography.

Antiviral and Cytotoxic Evaluation of Cyclopeptides 1-8 and Ternatin. The isolated natural ternatin **(9)**, not being of sufficient purity for biological evaluation, was synthesized following a modified version of the procedure described in the literature.[33,34] To assess the therapeutic potential of the isolated cyclopeptides, we evaluated their cytotoxicity and antiviral activity in three ZIKV-permissive cell lines: Vero E6, A549, and Huh7.5. Vero E6 is a non-cancerous African green monkey kidney epithelial cell line known for its high permissivity to arboviruses due to its deficient interferon response. A549 and Huh7.5 are human epithelial carcinoma-derived cell lines (lung and hepatocellular carcinoma, respectively). The cytotoxicity of comptonellins A-H and synthetic ternatin was evaluated using a mitochondrial activity assay after 48 h of treatment (**Figure 3A-C**). Compounds **2** and **8** displayed the lowest cytotoxicity across all cell lines, with CC_{50} values exceeding 30 µM in Vero E6 and above 5 µM in A549 and Huh7.5 cells (**Table 4**). Compounds **1** and **3** were the most cytotoxic, with CC_{50} values in the nanomolar range for A549 and Huh7.5. Ternatin displayed an intermediate cytotoxicity profile, with CC_{50} values of 4 µM in Vero E6 and 0.4 µM in A549 cells (**Table 4**). The

cytotoxicity data revealed striking differences among the tested cell lines. Comptonellins A and C exhibited pronounced cytotoxicity against the human cancer-derived cell lines A549 and Huh7.5, demonstrating over 450-fold and 130-fold higher cytotoxicity in A549 cells compared to Vero E6, respectively. Similarly, in Huh7.5 cells, their cytotoxicity was 20-fold and 2,000-fold greater than in Vero E6 cells. This selective cytotoxicity suggests a potential interaction with cellular pathways that are differentially regulated in cancerous versus non-cancerous cells.

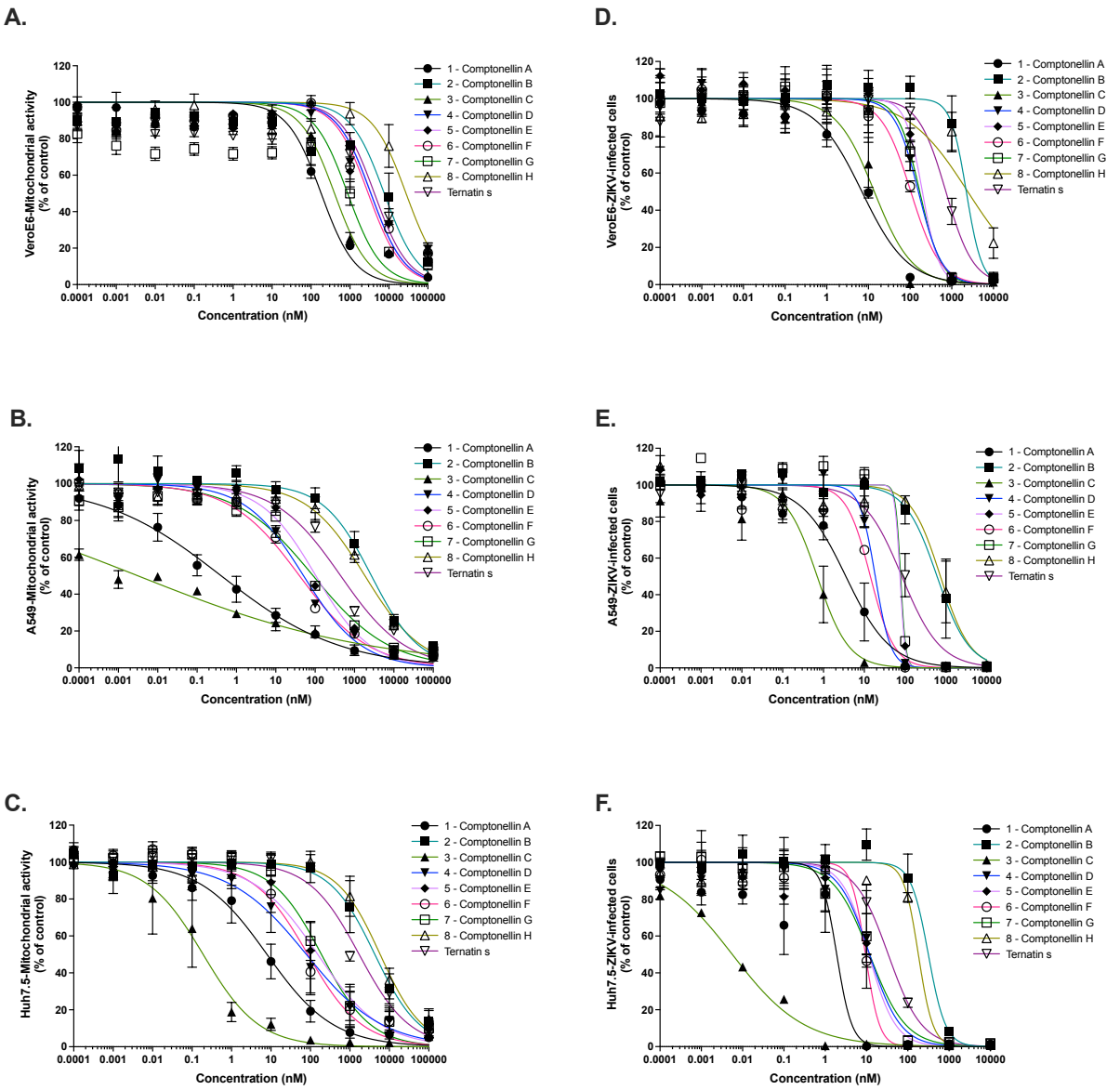

Figure 3. Investigation of the cytotoxicity and antiviral activity of compounds **1-8** and ternatin. (**A-C**) Mitochondrial activity of Vero E6 (**A**), A549 (**B**), and Huh7.5 (**C**) cells following

treatment with two-fold serial dilutions (0.0001–100,000 nM) of compounds **1**-**8** and ternatin for 48 h. Cytotoxicity was assessed using an MTT assay, and data are expressed as mean ± SD from three independent experiments, normalized to mock-treated controls.

(**D**-**F**) Antiviral activity of compounds **1**-**8** and ternatin against ZIKV in Vero E6 (**D**), A549 (**E**), and Huh7.5 (**F**) cells. Cells were infected with $ZIKV^{GFP}$ at an MOI of 1 and simultaneously treated with varying concentrations (0.0001–10,000 nM) of the compounds. Viral replication was quantified by flow cytometry analysis of GFP-positive cells at 24 h post-infection. Results are presented as mean ± SD from three independent experiments.

Table 4. Antiviral and Cytotoxic Activities of Compounds **1**-**8** and Ternatin.

Compound	Vero E6			A549			Huh7.5		
	CC_{50}[a]	IC_{50}[a]	SI[b]	CC_{50}[a]	IC_{50}[a]	SI[b]	CC_{50}[a]	IC_{50}[a]	SI[b]
Comptonellin A	182 ± 53	7 ± 3	26	0.4 ± 0.2	4 ± 2	< 1	8 ± 5	2 ± 0.5	4
Comptonellin B	7,118 ± 1,100	2,234 ± 600	3	2,694 ± 1,500	605 ± 225	4	4,279 ± 1,500	315 ± 35	14
Comptonellin C	400 ± 150	14 ± 9	29	0.003 ± 0.002	1 ± 0.4	< 1	0.2 ± 0.01	0.006 ± 0.002	35
Comptonellin D	3,087 ± 1,200	158 ± 63	20	51 ± 19	19 ± 5	3	79 ± 18	12 ± 7	7
Comptonellin E	3,123 ± 1,800	240 ± 74	13	104 ± 32	50 ± 18	2	153 ± 26	11 ± 5	13
Comptonellin F	2,720 ± 780	104 ± 51	26	40 ± 13	14 ± 6	3	86 ± 16	9 ± 2	9
Comptonellin G	860 ± 120	170 ± 32	5	89 ± 39	78 ± 36	1	190 ± 40	12 ± 8	16
Comptonellin H	30,377 ± 1,800	2,426 ± 315	13	1,842 ± 750	732 ± 250	3	5,840 ± 1,060	180 ± 45	32
Ternatin	3,904 ± 1050	723 ± 350	5	445 ± 120	83 ± 25	5	1,714 ± 415	34 ± 12	51

[a]Data in nM. Values are expressed as mean ± standard deviation calculated from three independent experiments. [b]Selectivity Index is calculated as CC_{50}/IC_{50}.

The antiviral activity of compounds **1**-**8** and ternatin was evaluated in ZIKV-infected Vero E6, A549, and Huh7.5 cells using $ZIKV^{GFP}$ infectious molecular clone (**Figure 2D-F**). Compounds **1** and **3** exhibited the strongest antiviral activity with IC_{50} values of 7 and 14 nM, respectively. Compounds **4**-**7** and ternatin showed strong antiviral effect, with IC_{50} values ranging from 104 to 240 nM, whereas compounds **2** and **8** were less efficient with IC_{50} values in the micromolar

range (**Table 4**). Despite exhibiting lower antiviral potency, compound **8** showed reduced cytotoxicity across all tested cell lines, resulting in selectivity indices of 13 in Vero E6 and 32 in Huh7.5 cells. The structural variations among the cyclopeptides significantly impact their antiviral efficacy. It seems that the presence of a hydroxy or hydroxy-formyl group on the amino acid at position 3 is detrimental to antiviral efficacy. The activity difference between compounds **1** and **2** suggests that *N*-methylation of the amino acid at position 3 is essential for antiviral effect. The dhML residue at position 4 also appears to enhance antiviral properties, as evidenced by the much higher efficacy of **1** versus ternatin. The absence of this residue in **8**, together with the presence of the hydroxylated residue in position 3 could explain the lower efficacy of compound **8**.

The antiviral efficacy of compound **1** was evaluated against Dengue virus serotype 2 (DENV-2), Ross River virus (RRV), and SARS-CoV-2, in comparison to ternatin (**Figure 4**). Representative flow cytometry plots illustrating the dose-dependent antiviral activity of comptonellin A (compound **1**) against DENV-2 and SARS-CoV-2 are provided in **Figures S87** and **S88**. Our data demonstrate that compound **1** exhibits potent, dose-dependent inhibition of DENV-2 replication, achieving complete viral suppression at 100 nM, with an IC_{50} value of 31 nM and an SI of approximately 6. In contrast, ternatin required concentrations approximately one log higher to elicit a comparable response (**Figure 4A**). Similarly, compound **1** effectively inhibited RRV replication, with an IC_{50} of 45 nM (SI 4.0), although slightly higher concentrations were necessary compared to DENV-2, suggesting a broad-spectrum antiviral potential against medically relevant arboviruses (**Figure 4B**). Notably, compound **1** also displayed significant inhibitory activity against SARS-CoV-2 with an IC_{50} of 31 nM and an SI of 6 (**Figure 4C**), further reinforcing its broad-spectrum antiviral properties across distinct viral families. In contrast, ternatin exhibited only modest effects against SARS-CoV-2, underscoring the enhanced potency of compound **1**. These findings suggest that compound **1** likely exerts its

antiviral effects through a host-directed mechanism, targeting cellular pathways essential for the replication of diverse RNA viruses, rather than directly interacting with viral proteins.

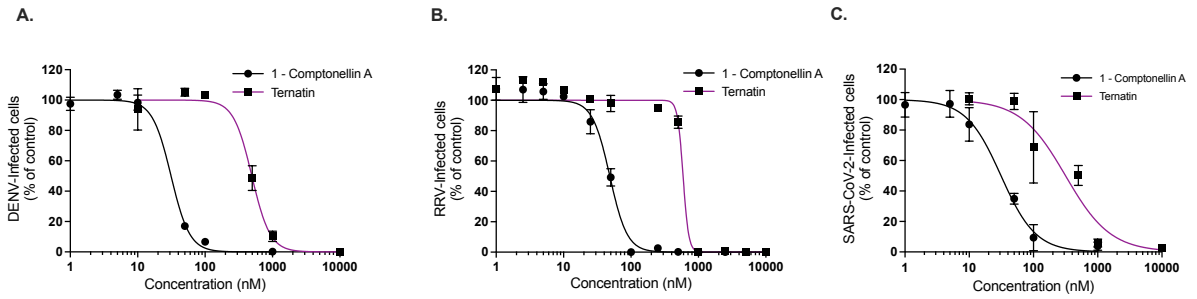

Figure 4. Broad-spectrum antiviral activity of compound **1** against DENV-2, RRV, and SARS-CoV-2. (**A-C**) Vero E6 cells were infected with Dengue virus serotype 2 (DENV-2) (**A**), Ross River virus (RRV) (**B**), and SARS-CoV-2 (**C**) at an MOI of 0.1 and simultaneously treated with increasing concentrations (1-10,000 nM) of compound **1** or ternatin. Viral replication was monitored using flow cytometry analysis of 4G2-labeled cells (DENV-2, **A**), luminescence quantification of RRV-Luc-expressing cells (**B**), and flow cytometry detection of anti-Spike-labeled cells (SARS-CoV-2, **C**). Data are expressed as mean ± SD from three independent experiments, normalized to untreated infected controls.

The series of compounds isolated in this study represents an uncommon structural class related to ternatin, first isolated in 1974 from a culture of the fungus *Didymocladium ternatum* (Bonord.) sacc.[35] Subsequent studies have reported ternatin in other fungal species, suggesting that the comptonellins described in this study may have an endophytic origin.[31,36,37] Since the discovery of ternatin, only five natural analogues, isolated from an endophytic fungus of *Garcinia scortechinii*, have been described. The five compounds also contain seven amino acids, several of which are *N*-methylated, as well as non-canonical residues such as dhML and unnatural D-series amino acids. They all feature a D-pipecolic acid in position 6, which is

specific to this series of analogues. The authors report their cytotoxic properties on several cancer cell lines.[32] Ternatin and synthetic derivatives have also been studied for their antibacterial, anti-adipogenesis, and anticancer properties.[31,32,34–36,38–45] A significant breakthrough in recent years has been the identification of ternatin and its analogues as potent inhibitors of the eukaryotic elongation factor-1A (eEF1A), a key component of the cellular translation machinery.[34] eEF1A is essential for delivering aminoacyl-tRNAs to the ribosomal A-site during protein synthesis. It is a crucial node for viral replication, particularly for RNA viruses that rely heavily on the host translation machinery. Studies on ternatin and its improved synthetic variants have demonstrated their ability to bind competitively to eEF1A, thereby interfering with mRNA translation and protein synthesis. For example, ternatin-4, a ternatin variant comprising both dhML and pipecolic acid, was shown to possess potent anti-SARS-CoV-2 effects, disturbing viral protein production.[46] This aligns with our findings, which strongly suggest that comptonellins A and C may act through a similar mechanism, effectively disrupting viral replication by targeting eEF1A. This host-targeted mode of action has profound implications for antiviral drug development. Plitidepsin, a marine-derived didemnin analogue, has demonstrated remarkable activity against SARS-CoV-2, outperforming remdesivir in preclinical models by binding to eEF1A and disrupting viral translation.[47] In a recent study, Molina *et al*. (2025) further demonstrated that plitidepsin selectively impairs cap-dependent and IRES-mediated translation of viral RNAs, while affecting less than 13% of the host proteome, thus preserving cellular viability.[48] Their findings support the concept that eEF1A-targeting agents can achieve broad-spectrum antiviral efficacy without widespread cytotoxicity, validating host translation machinery as a viable therapeutic target. Similarly, didemnin B and ternatin-4 inhibit conformational changes in eEF1A required for aminoacyl-tRNA accommodation into ribosomes, leading to translation arrest. Given these findings, our study suggests that comptonellins may act in an analogous manner, targeting host-cell translation

factors rather than viral components, thereby inhibiting replication across multiple medically relevant arboviruses, including Zika, Dengue-2, and Ross River virus.

The potential broad-spectrum activity of eEF1A inhibitors extends beyond orthoflaviviruses and alphaviruses, as evidenced by the inhibition of SARS-CoV-2 by comptonellin A. This further supports the idea that host-directed antivirals targeting essential cellular pathways can provide effective countermeasures against diverse viral families. Given these insights, the comptonellins described in this study serve as promising scaffolds for further optimization in medicinal chemistry. Future work should focus on elucidating their precise binding interactions with eEF1A, evaluating their antiviral spectrum across additional RNA viruses, and assessing their pharmacokinetic properties for potential therapeutic development.

EXPERIMENTAL SECTION

General Experimental Procedures. Optical rotations were measured at 20 °C on an Anton Paar MCP 300 polarimeter. NMR spectra of compounds **1**-**9** were recorded on a Bruker 700 MHz instrument (Avance 700). Chemical shifts (relative to CD_3CN) are in ppm and coupling constants are in Hz. Nucleodur analytical and semi-preparative C_{18} columns (250 × 4.6 mm and 250 × 10 mm; 5 μm, Macherey-Nagel) were used for HPLC separations using a Waters autopurification system equipped with a sample manager (Waters 2767), a column fluidics organizer, a binary pump (Waters 2525), a UV–vis diode array detector (190–600 nm, Waters 2996), and a PL-ELS 1000 ELSD Polymer Laboratory detector. HRESIMS data were acquired using an Acquity Waters UPLC coupled to a Waters LCT Premier XE mass spectrometer. The ionization was carried out using an electrospray ionization source in the positive mode (range *m/z* 80−1500). All solvents were purchased from Carlo Erba (France) or SDS (Peypin, France) and analytical plates (Si gel 60 F254) were from Merck (France). Prepacked Flash Pur EcoFlex

Büchi (France) silica gel (50 µm, irregular) cartridge was used for flash chromatography using a Teledyne Isco Combiflash Rf 200i.

Plant Material. Bark of *Comptonella drupacea* (Labill.) Guillaumin was collected in May 2008 by Cyril Poullain in « Réserve spéciale de faune du col d'Amieu et Table Unio », South Province, New Caledonia and authenticated by Jean-Marie Veillon (IRD). The collection was carried out under the collection authorization n°6024-597-2008/DENV/SMT. The corresponding voucher specimen POU-0234 has been deposited at the Herbarium of the IRD Center, Nouméa, New Caledonia. Bark was dried at a temperature not exceeding 40 °C using a hot air generator before being ground and stored at room temperature.

Extraction and Isolation. Ground bark (0.24 kg) of *Comptonella drupacea* was extracted with EtOAc (4 X 0.5 L, 1 h each, 35 °C) to yield 4.0 g of crude extract after concentration *in vacuo*. The residue was subjected to a 220 g silica gel column flash chromatography using a gradient of *n*-heptane/EtOAc/MeOH of increasing polarities (100:0:0 to 0:100:0 in 16 CV to 0:70:30 in 8 CV, 80 mL.min^{-1}) to afford 12 fractions, F1-F12, according to their TLC profiles. F11 (750 mg) was purified by preparative HPLC (Nucleodur C_{18}, 10 mM ammonium acetate buffer-CH_3CN, 90:10 to 10:90 at 21 mL.min^{-1}) to yield 3 subfractions of which subfraction 3 contained compound **1** (8.0 mg, t_R 30.5 min). Cleared of **1**, subfraction 3 (119 mg) was further purified (preparative HPLC, Nucleodur C_{18}, 10 mM ammonium acetate buffer/CH_3CN, 50:50 to 30:70 at 21 mL.min^{-1}) to afford **2** (2.9 mg, t_R 15.8 min), **9** (2.0 mg, t_R 19.0 min) and **3** (2.7 mg, t_R 25.3 min). F12 (278 mg) was subjected to preparative HPLC (Nucleodur C_{18}, 10 mM ammonium acetate buffer-CH_3CN, 50:50 to 30:70 at 21 mL.min^{-1}) to yield **4** (5.3 mg, t_R 15.4 min), **5** (1.7 mg, t_R 17.5 min), **6** (2.5 mg, t_R 26.5 min), **7** (0.7 mg, t_R 29.7 min) and **8** (1.6 mg, t_R 13.7 min).

*Comptonellin A (**1**)*. Yellow amorphous solid; $[\alpha]_D^{20}$ - 33.2° (*c* 0.4, EtOH); ^{1}H and ^{13}C NMR, see **Table 1**; HRESIMS *m/z* 750.5121 $[M+H]^+$ (calcd for $C_{38}H_{68}N_7O_8^+$ 750.5124), *m/z* 772.4938 $[M + Na]^+$ (calcd for $C_{38}H_{67}N_7O_8Na^+$ 772.4943). NP-MRD ID: NP0350688. GNPS ID: CCMSLIB00013580750 $[M+H]^+$, CCMSLIB00013580889 $[M+Na]^+$.

*Comptonellin B (**2**)*. Yellow amorphous solid; $[\alpha]_D^{20}$ – 6.0° (*c* 0.3, EtOH); ^{1}H and ^{13}C NMR, see **Table 1**; HRESIMS *m/z* 736.4971 $[M+H]^+$ (calcd for $C_{37}H_{66}N_7O_8^+$ 736.4967), *m/z* 758.4802 $[M + Na]^+$ (calcd for $C_{37}H_{65}N_7O_8Na^+$ 758.4787). NP-MRD ID: NP0350689. GNPS ID: CCMSLIB00013580890 $[M+H]^+$, CCMSLIB00013580892 $[M+Na]^+$.

*Comptonellin C (**3**)*. Yellow amorphous solid; $[\alpha]_D^{20}$ – 10.2° (*c* 0.4, EtOH); ^{1}H and ^{13}C NMR, see **Table 1**; HRESIMS *m/z* 764.5279 $[M+H]^+$ (calcd for $C_{39}H_{70}N_7O_8^+$ 764.5280), *m/z* 786.5105 $[M + Na]^+$ (calcd for $C_{39}H_{69}N_7O_8Na^+$ 786.5100). NP-MRD ID: NP0350690. GNPS ID: CCMSLIB00013580893 $[M+H]^+$, CCMSLIB00013580894 $[M+Na]^+$.

*Comptonellin D (**4**)*. Yellow amorphous solid; $[\alpha]_D^{20}$ – 16.5° (*c* 0.4, EtOH); ^{1}H and ^{13}C NMR, see **Table 2**; HRESIMS *m/z* 766.5106 $[M+H]^+$ (calcd for $C_{38}H_{68}N_7O_9^+$ 766.5073), *m/z* 788.4963 $[M + Na]^+$ (calcd for $C_{38}H_{67}N_7O_9Na^+$ 788.4892). NP-MRD ID: NP0350691. GNPS ID: CCMSLIB00013580895 $[M+H]^+$, CCMSLIB00013580896 $[M+Na]^+$.

*Comptonellin E (**5**)*. Yellow amorphous solid; $[\alpha]_D^{20}$ – 13.2° (*c* 0.4, EtOH); ^{1}H and ^{13}C NMR, see **Table 2**; HRESIMS *m/z* 780.5248 $[M+H]^+$ (calcd for $C_{39}H_{70}N_7O_9^+$ 780.5230), *m/z* 802.5085 $[M + Na]^+$ (calcd for $C_{39}H_{69}N_7O_9Na^+$ 802.5049). NP-MRD ID: NP0350692. GNPS ID: CCMSLIB00013580897 $[M+H]^+$, CCMSLIB00013580898 $[M+Na]^+$.

*Comptonellin F (**6**)*. Yellow amorphous solid; $[\alpha]_D^{20}$ – 21.5° (*c* 0.4, EtOH); ^{1}H and ^{13}C NMR, see **Table 2**; HRESIMS *m/z* 794.5013 $[M+H]^+$ (calcd for $C_{39}H_{68}N_7O_{10}^+$ 794.5022). NP-MRD ID: NP0350693. GNPS ID: CCMSLIB00013580899 $[M+H]^+$, CCMSLIB00013580900 $[M+Na]^+$.

Comptonellin G (7). Yellow amorphous solid; $[\alpha]_D^{20}$ – 9.3° (*c* 0.3, EtOH); ^{1}H and ^{13}C NMR, see **Table 3**; HRESIMS *m/z* 808.5212 $[M+H]^+$ (calcd for $C_{40}H_{70}N_7O_{10}^+$ 808.5179), *m/z* 830.5160 $[M + Na]^+$ (calcd for $C_{40}H_{69}N_7O_{10}Na^+$ 830.4998). NP-MRD ID: NP0350694. GNPS ID: CCMSLIB00013580901 $[M+H]^+$, CCMSLIB00013580902 $[M+Na]^+$.

*Comptonellin H (**8**)*. Yellow amorphous solid; $[\alpha]_D^{20}$ – 9.0° (*c* 0.4, EtOH); ^{1}H and ^{13}C NMR, see **Table 3**; HRESIMS *m/z* 754.5084 $[M+H]^+$ (calcd for $C_{37}H_{68}N_7O_9^+$ 754.5073), *m/z* 776.4898 $[M + Na]^+$ (calcd for $C_{37}H_{67}N_7O_9Na^+$ 776.4892). NP-MRD ID: NP0350695. GNPS ID: CCMSLIB00013580903 $[M+H]^+$, CCMSLIB00013580904 $[M+Na]^+$.

*Ternatin (**9**)*. Yellow amorphous solid; $[\alpha]_D^{20}$ – 33.2° (*c* 0.4, EtOH); HRESIMS *m/z* 738.5154 $[M+H]^+$ (calcd for $C_{37}H_{68}N_7O_8^+$ 738.5124), *m/z* 760.4983 $[M + Na]^+$ (calcd for $C_{37}H_{67}N_7O_8Na^+$ 760.4943). GNPS ID: CCMSLIB00013580905 $[M+H]^+$, CCMSLIB00013580906 $[M+Na]^+$.

Marfey's Analysis. Compound **1** (0.4 mg) was dissolved in 6 N aqueous HCl (200 µL) and stirred at 100 °C for 15 h. The hydrolyzed solution was evaporated to dryness and dissolved in 100 µL H_2O. To the solution was added 100 µL of 25 mM FDAA in acetone and 20 µL of 1 M aqueous $NaHCO_3$ solution. The mixture was heated at 45 °C for 45 min. The reaction was quenched with 20 µL of 1 N aqueous HCl solution, diluted with 900 µL of HPLC-grade CH_3CN and filtered. Each amino acid standard (0.5 mg) was dissolved in 100 µL H_2O and derivatized in the same manner. All derivatives were analysed by UPLC-MS at 50 °C using a BEH Premier C_{18} (2.1x100 mm, 1.7 µm) column and a gradient of H_2O-MeOH + 0.1 % formic acid, 75:25 (0-0.5 min) to 50:50 (0.5-16 min). The retention times of the derivatized amino acid standards were as follows: (*N*Me)-L-Ala (4.05 min), (*N*Me)-D-Ala (4.60 min), (*N*Me)-L-Leu (12.35 min), (*N*Me)-D-Leu (14.70 min), L-*threo*-OH-Leu (4.25 min), D-*threo*-OH-Leu (10.75 min), L-Ile (8.30 min), D-Ile (14.90 min), D-*allo*-Ile (14.90 min). The retention times of the acid hydrolysate derivatives of **1** were as follows: (*N*Me)-L-Ala (4.05 min), (*N*Me)-D-Ala (4.60

min), in proportion L/D, 2/1, (*N*Me)-L-Leu (12.35 min), D-OH-Leu (9.80 min), D-*allo*-Ile (14.9 min) (**Figure S21)**.

Data-Dependent LC-ESI-HRMS^2 Analysis.

LC analyses were performed using a Thermo Ultimate 3000 system equipped with a Cortecs C_{18} column (2.1 × 100 mm; 2.7 µm, Waters). The mobile phase consisted of water-acetonitrile (H_2O-CH_3CN) acidified with 0.1% formic acid (90:10) held for 2 min, then a gradient from 90:10 to 0:100 in 20 min held at 0:100 for 8 min at a flow rate of 600 µL.min^{-1}. The temperature of the column oven was set to 40 °C, and the injection volume was set to 5 µL. LC-ESI-HRMS^2 analyses were achieved by coupling the LC system to an Impact II Bruker quadrupole time-of-flight mass spectrometer (Bruker Daltonics, Bremen, Germany) equipped with an ESI dual source (operating in the positive-ion mode). Source parameters were set as follows: end plate offset-350 V, capillary voltage-4,500 V, nebulizer pressure-60 psi, drying gas flow rate-10 L.min^{-1}, drying gas temperature-240 °C. MS scans were operated in full-scan mode from *m*/*z* 100 to 1,400 (at 6 Hz). MS^1 scan was followed by MS^2 scans of the five most intense ions above an absolute threshold of 2,000 counts. Selected parent ions were fragmented with a collision energy fixed at 30 eV and using an *m*/*z* dependent isolation window of 2-4 amu**.** The mass accuracy was guaranteed via an injection of a calibration solution from sodium formate clusters with external (at the beginning of each run) and internal (segment 0.1 at 0.4 min of each sample) calibration by a High Precision Calibration (HPC) equation with a maximum mass delta of 1 ppm and 7 as the minimal number of calibration points. LC-UV and MS data acquisition and processing were performed using DataAnalysis 4.4 software (Bruker Daltonics, Bremen, Germany).

Data Preprocessing. Raw data were converted into .mzML format using DataAnalysis 4.4 software. All .mzML files were modified using the precursor *m/z* value corrector provided by Garayev *et al*.[49], then processed using MZmine 4.1.0.[28]

Mass detection was conducted using a noise level of 800 counts for MS and 100 counts for MSMS dimension. The LC-MS chromatogram builder was used with a minimum consecutive scans of 4, a minimum intensity for consecutive scans of 3,000, a minimum absolute height of 3,500, and an *m/z* tolerance of 10 ppm.[50] The local minimum feature resolver was used with the following standard settings: chromatographic threshold, 80%; minimum search range RT (absolute), 0.06; minimum absolute height, 3,500; minimum ratio of peak top/edge, 1.8; peak duration range (min), 0.0-2.0; minimum scans, 4. However, considering the diverse molecular contents of extracts included within this wide-ranging collection, these peak-picking parameters needed to be reoptimized for a few specific samples showing divergent chromatographic profiles and peak shapes.

MS2 scans were paired using MS1 to MS2 precursor tolerance of 20 ppm and feature edges were used as RT filter. Isotopologues were grouped using the ^{13}C isotope filter with an *m/z* tolerance of 5 ppm, an RT tolerance of 0.03 min, a monotonically decreasing isotope pattern, a maximum charge of 2 and the most intense peak as the representative isotope. Further isotope signals were searched with the isotopic peaks finder module with an *m/z* tolerance of 5 ppm. Peak alignment was performed using the join aligner module (*m/z* tolerance, 7 ppm; weight for *m/z*, 1; RT tolerance, 0.1 min; weight for RT, 1). The feature list was filtered to retain only rows that contain MS2 scan and was gap-filled with the peak finder module (*m/z* tolerance, 4 ppm; RT tolerance, 0.05 min; minimum scans, 4). The duplicate peak filter was applied (*m/z* tolerance, 2 ppm; RT tolerance, 0.03 min). Ion adducts were then identified using the metaCorrelate feature grouping and ion identity networking modules.[51]

Eventually, the .mgf and .csv files needed for subsequent molecular networking and annotation were exported using the dedicated "Export molecular networking files" and "Export for Sirius" modules.

Molecular Network Analysis. The .mgf spectral data and .csv files for molecular networking were imported into MetGem 1.5.2.[29] The *m/z* tolerance window used to find matching peaks was set to 0.005 Da, and cosine scores were kept under consideration for spectra sharing at least 5 matching peaks. MS2 spectra were filtered by keeping peaks higher than 50 Da and by choosing the top 10 peaks within the ±50 Da window throughout the spectrum. The t-SNE networks were created with nodes sharing at least 8 cosine scores above 0.6 with others. The number of iterations, perplexity, learning rate, and early exaggeration parameters were set to 100 000, 12, 200, and 12, respectively. The Barnes-Hut approximation was enabled and an angle of 0.2 was applied. The t-SNE output was imported into Cytoscape 3.10.2 for advanced network visualization and image export.[52]

Compound Annotation. The metabolite annotation was performed in MetGem by searching for GNPS MS/MS spectral library matches (https://gnps.ucsd.edu/ProteoSAFe/libraries.jsp). The spectral data corresponding to the ion clusters of interest were selected from the .mgf file for Sirius and imported into Sirius 6.0.0 for computing using the Molecular Formula Identification, CSI:FingerID (fingerprint prediction) and Canopus (compound class prediction) modules.[30,53–58] The MS^2 mass accuracy was set to 5 ppm, and the bio databases were considered for structure prediction.

Ternatin Synthesis. Ternatin was synthesized following a modified version of the procedure described by J. Taunton.[33,34] The synthesis was carried out manually using Fmoc/tBu strategy

in a polypropylene reaction vessel fitted with polyethylene frits. Carboxylic acid C_{term} ternatin was synthesized on 2-chlorotritylchloride resin (polystyrene) (theoretical loading of 1.6 mmol/g – 100-300 mg). After swelling of the resin for 15 min in CH_2Cl_2, the first amino acid, Fmoc-*β*-OH-D-Leu was loaded through nucleophilic substitution by shaking the resin in a solution of Fmoc-*β*-OH-D-Leu (0.8 mmol/g) and DIPEA (1.5 equiv.) in anhydrous CH_2Cl_2 (10 mL/g resin) for 30 min at room temperature. The unreacted sites were then capped by shaking the resin in a mixture of MeOH/DIPEA/CH_2Cl_2 (2/1/17 v/v/v; 10.0 mL/g resin) for 10 min (repeated two times). The resin was then washed two times with DMF and three times with CH_2Cl_2 (10.0 mL/g resin) for 30 sec. The overall process yielded a resin loading of around 0.5 mmol/g. The elongation of the peptide was performed by cycle repetition of peptide coupling and Fmoc removal using 1) Fmoc-D-*N*Me-Ala, 2) Fmoc-L-*N*Me-Ala, 3) Fmoc-L-Leu, 4) Fmoc-L-*N*Me-Leu, 5) Fmoc-L-*N*Me-Ala, and 6) Fmoc-D-*allo*-Ile. Cleavage of the linear peptide from the resin was carried out with HFIP before peptide cyclization in the presence of PyAOP. After purification on reverse phase chromatography and lyophilization, the desired ternatin (4.5 mg, 0.006 mmol, 41%) was isolated with purity >99% (determined by UPLC-UV). All spectral data (NMR and HRMS) were in accordance with those reported for ternatin.[39,45]

Fmoc removal procedure: *N*-*α*-Fmoc protecting groups were removed by shaking the resin in piperidine/DMF solution (1/4, v/v; 10.0 mL/g resin) for 5 min at room temperature. The process was repeated two times for 10 min, and the completeness of deprotection was monitored by ultraviolet absorption measurement of the filtrate at 299 nm. The resin was then washed five times with DMF and once with CH_2Cl_2 (10.0 mL/g resin) for 30 sec.

Coupling procedure: Coupling reactions were performed by shaking the resin with a solution of *N*-*α*-Fmoc-protected amino acid (2.0 equiv.), HATU (1.9 equiv.) and DIPEA (4.0 equiv.) in DMF (10.0 mL/g resin) for 30 min at room temperature. The 5th Fmoc-protected amino acid

was introduced using PyAOP (1.9 equiv.) instead of HATU. Completeness of the coupling was controlled by TNBS or Chloranil test.

Resin cleavage procedure: The resin was first washed five times with CH_2Cl_2 (10.0 mL/g resin) before shaking in a mixture of 20% HFIP in DCM (10.0 mL/g resin) for 20 min at room temperature and then filtrated. The resin was rinsed once with the same mixture for 1 min. The recovered solutions were concentrated under reduced pressure.

Cyclization procedure: Crude linear peptide was dissolved in DMF (0.50 mM) with 2.5 equiv. of DIPEA. PyAOP (1.1 equiv.) was added, and the solutions were stirred at room temperature for 1 h. Solvent was removed under reduced pressured.

Purification procedure: Ternatin was purified by RP-C18 flash chromatography using eluent composed from 5% ACN+0.1% TFA to 70% ACN+0.1% TFA.

Cells, Viruses and Reagents. Vero E6 (ATCC, CCL-81), A549 (ATCC, CCL-185), and Huh7.5 cells (generous gift from Dr. Claudia dos Santos, Fiocruz, Brazil) were maintained in Dulbecco's Modified Eagle Medium (DMEM) supplemented with 10% fetal bovine serum (FBS), 2 mM L-glutamine, 1 mM sodium pyruvate, and a mix of antibiotics including 100 U/mL penicillin, 0.1 mg/mL streptomycin, and 0.5 µg/mL fungizone. The viruses used in this study included $ZIKV^{GFP}$, Dengue virus serotype 2 (DENV-2), Ross River virus (RRV),[59] and SARS-CoV-2.[60] ZIKV-GFP was derived from the MR766NIID strain using the Infectious Subgenomic Amplicons (ISA) method.[26] DENV-2 was a clinical isolate from the 2022 outbreak in Réunion Island. RRV replication was assessed using a luciferase-expressing molecular clone (RRV^{LUC}), allowing for luminescence-based quantification of viral infection. SARS-CoV-2 was a clinical isolate propagated in Vero E6 cells, with viral stocks generated from infected cultures displaying cytopathic effects three days post-infection. Viral stocks titration was performed using the plaque-forming unit (PFU) assay. Vero E6 cells were seeded in 24-well

plates at 70,000 cells per well and infected with serial tenfold dilutions of viral stocks. After two hours of virus adsorption, cells were overlaid with 1% carboxymethyl cellulose in DMEM supplemented with 5% FBS, restricting viral spread. Three days post-infection, cells were fixed with 3.7% paraformaldehyde (PFA) and stained with 0.1% crystal violet in 20% ethanol to visualize plaques.

Mitochondrial Activity Assay. Cells were seeded in 96-well plates at a density of 1.5×10^4 cells per well and exposed to ten-fold serial dilutions of compounds. After a 48 h-incubation at 37 °C, cells were washed with 1X PBS, and 120 µL of fresh culture medium containing 5 mg/mL MTT (3-[4,5-dimethylthiazol-2-yl]-2,5-diphenyltetrazolium bromide) was added to each well. The plates were further incubated for 2 h to allow for formazan crystal formation. Subsequently, the MTT-containing medium was removed, and the crystals were solubilized by adding 50 µL of dimethyl sulfoxide (DMSO). The absorbance was recorded at 570 nm, with a reference wavelength of 690 nm for background correction.

Antiviral Assay. To evaluate the antiviral activity of the compounds, cells were seeded in 96-well plates and incubated overnight at 37 °C in a humidified atmosphere containing 5% CO_2. The following day, cells were simultaneously exposed to serial dilutions of each compound (0.0001-10,000 nM for ZIKV assays; 1-10,000 nM for DENV-2, RRV, and SARS-CoV-2 assays) and infected with the respective viruses. All assays were performed in triplicate.

For Zika virus, A549, Huh7.5, and Vero E6 cells were infected with a GFP-expressing clone ($ZIKV^{GFP}$) derived from the MR766 strain at a multiplicity of infection (MOI) of 1. After 24 hours of co-treatment and infection, cells were fixed with 3.7% paraformaldehyde and analyzed by flow cytometry to quantify GFP-positive infected cells.

For Dengue virus serotype 2 (DENV-2), SARS-CoV-2, and Ross River virus (RRV^{LUC}), antiviral activity was evaluated exclusively in Vero E6 cells. For DENV-2, cells were infected at an MOI of 0.1 and co-treated with compounds. Forty-eight hours post-infection, cells were fixed and stained with the pan-flavivirus monoclonal antibody 4G2 conjugated to Alexa Fluor 488 (1:1000 in PBS containing 2% BSA), then analyzed by flow cytometry.

For SARS-CoV-2, cells were infected with a clinical isolate at an MOI of 0.1 and co-treated with compounds. After 48 hours, cells were fixed and incubated for 1 hour with with a monoclonal human IgG1 anti-Spike antibody (clone H4) purchased from InvivoGen (Toulouse, France), followed by a goat anti-human Alexa Fluor 488-conjugated secondary antibody (ThermoFisher, 1:1000). Labeled cells were analyzed by flow cytometry.

For RRV-Luc, cells were infected with a luciferase-expressing recombinant virus at an MOI of 0.1 in the presence of compounds. After 24 hours, luminescence was measured using the Bright-Glo Luciferase Assay System (Promega) and normalized to untreated infected controls.

Flow Cytometry Assay. Cells were harvested, fixed with 3.7% paraformaldehyde (PFA) in PBS for 20 minutes, and processed using a CytoFLEX flow cytometer (Beckman Coulter). The percentage of infected cells was quantified by flow cytometry. A minimum of 2,000 events per sample was recorded. Gating was performed on singlet and live cell populations to quantify the percentage of infected cells. Data acquisition and analysis were performed using CytExpert software (version 9.00, La Jolla, CA, USA)**.**

IC_{50} and CC_{50} Determination. Cytotoxic concentration (CC_{50}) and inhibitory concentration (IC_{50}) values were determined through nonlinear regression analysis, generating sigmoidal dose-response curves performed in GraphPad Prism software. Data are presented as mean ± SD from at least three independent experiments performed in triplicate. CC_{50} values were

calculated relative to untreated (mock-treated) cells, while IC_{50} values were determined by comparing infected cells to untreated infected controls (mock-infected).

ASSOCIATED CONTENT

Data Availability Statement. Raw .d and .mzML files of the EtOAc bark extract of *Comptonella drupacea* have been deposited in the MassIVE data repository (MassIVE ID: MSV000097264). The NMR raw data files for comptonellins A-H have been deposited in The Natural Products Magnetic Resonance Database under the NP IDs NP0350688 to NP0350695. Comptonellins A-H and ternatin MS/MS spectra have been added to the GNPS Public Spectral Library.

Supporting Information. HRESIMS spectra of compounds **1**-**9**; MS/MS spectrum of **1**; 1D NMR (^{1}H, ^{13}C) and 2D NMR (COSY, TOCSY, HSQC-TOCSY, HSQC, HMBC, and ROESY) data for compounds **1**-**9**; UHPLC-MS analysis of Marfey's derivatives of **1**; Key ROESY correlations of **1**; TOCSY and HMBC correlations of amino acid residue[3] (**2**-**7**) and residues[3,4] (**8**); Representative flow cytometry plots for **1**. (PDF)

AUTHOR INFORMATION

Corresponding Authors.

Cécile Apel-*Université Paris-Saclay, CNRS, Institut de Chimie des Substances Naturelles, UPR 2301, 91198, Gif-sur-Yvette, France*

*Tel: +33 1 69 82 30 38. E-mail: cecile.apel@cnrs.fr

ORCID: 0000-0003-3785-9620

Chaker El Kalamouni-*Unité Mixte Processus Infectieux en Milieu Insulaire Tropical, Université de la Réunion, INSERM U1187, CNRS UMR 9192, IRD UMR 249, Plateforme Technologique CYROI, 94791 Sainte Clotilde, France*

*Tel: +262 262 93 91 95. E-mail: chaker.el-kalamouni@univ-reunion.fr

ORCID: 0000-0003-4673-6614

Marc Litaudon-*Université Paris-Saclay, CNRS, Institut de Chimie des Substances Naturelles, UPR 2301, 91198, Gif-sur-Yvette, France*

*Tel: +33 1 69 82 30 38. E-mail: marc.litaudon@cnrs.fr

ORCID: 0000-0002-0877-8234

Authors.

Juliano Haddad-*Unité Mixte Processus Infectieux en Milieu Insulaire Tropical, Université de la Réunion, INSERM U1187, CNRS UMR 9192, IRD UMR 249, Plateforme Technologique CYROI, 94791 Sainte Clotilde, France*

Charline Herrscher-*Unité Mixte Processus Infectieux en Milieu Insulaire Tropical, Université de la Réunion, INSERM U1187, CNRS UMR 9192, IRD UMR 249, Plateforme Technologique CYROI, 94791 Sainte Clotilde, France*

Clément Grisel-*Université Paris-Saclay, CNRS, Institut de Chimie des Substances Naturelles, UPR 2301, 91198, Gif-sur-Yvette, France*

Justine Girard-*Unité Mixte Processus Infectieux en Milieu Insulaire Tropical, Université de la Réunion, INSERM U1187, CNRS UMR 9192, IRD UMR 249, Plateforme Technologique CYROI, 94791 Sainte Clotilde, France*

Florent Olivon-*Université Paris-Saclay, CNRS, Institut de Chimie des Substances Naturelles, UPR 2301, 91198, Gif-sur-Yvette, France*
ORCID: 0000-0002-3662-5390

Cyril Poullain-*Laboratoire de Chimie Bio-inspirée et d'Innovations Ecologiques, ChimEco, UMR 5021 CNRS – UM, Cap Delta, 1682 Rue de la Valsière, 34790 Grabels, France*

Jean-François Gallard-*Université Paris-Saclay, CNRS, Institut de Chimie des Substances Naturelles, UPR 2301, 91198, Gif-sur-Yvette, France*

Stéphanie Boutet-*Institut Jean-Pierre Bourgin (IJPB), AgroParisTech, INRAE, Université Paris-Saclay, 78000, Versailles, France*

Fanny Roussi-*Université Paris-Saclay, CNRS, Institut de Chimie des Substances Naturelles, UPR 2301, 91198, Gif-sur-Yvette, France*

Sandy Desrat-*Université Paris-Saclay, CNRS, Institut de Chimie des Substances Naturelles, UPR 2301, 91198, Gif-sur-Yvette, France*
ORCID: 0000-0002-6544-9242

Notes. Some of the findings reported in this study are disclosed in Patent application No. WO2024231530, EP4461367. **Figures S4-11** and **Tables 1-3** have been reproduced or adapted from this patent.

The authors declare no competing financial interest.

ACKNOWLEDGMENTS

The authors are very grateful to the South Province of New Caledonia, which has facilitated our field investigation. This work received financial support from POE FEDER 2014-20 of the Conseil Régional de La Réunion (ZIKAlert program, N° SYNERGIE: RE00001902), AxLR – SATT Occitanie Méditerranée, SATT Paris-Saclay, Université Paris-Saclay and the Agence Nationale pour la Recherche (ANR-11-IDEX-0003-02). This work has also benefited from the support of IJPB's Plant Observatory technological platforms funded by Saclay Plant Sciences-SPS (ANR-17-EUR-0007).

REFERENCES

(1) Challenges in Combating Arboviral Infections. *Nat. Commun.* **2024**, *15* (1), 3350. https://doi.org/10.1038/s41467-024-47161-3.

(2) Tatem, A. J.; Hay, S. I.; Rogers, D. J. Global Traffic and Disease Vector Dispersal. *Proc. Natl. Acad. Sci.* **2006**, *103* (16), 6242–6247. https://doi.org/10.1073/pnas.0508391103.

(3) Kilpatrick, A. M.; Randolph, S. E. Drivers, Dynamics, and Control of Emerging Vector-Borne Zoonotic Diseases. *The Lancet* **2012**, *380* (9857), 1946–1955. https://doi.org/10.1016/S0140-6736(12)61151-9.

(4) Bhatt, S.; Gething, P. W.; Brady, O. J.; Messina, J. P.; Farlow, A. W.; Moyes, C. L.; Drake, J. M.; Brownstein, J. S.; Hoen, A. G.; Sankoh, O.; Myers, M. F.; George, D. B.; Jaenisch, T.; Wint, G. R. W.; Simmons, C. P.; Scott, T. W.; Farrar, J. J.; Hay, S. I. The Global Distribution and Burden of Dengue. *Nature* **2013**, *496* (7446), 504–507. https://doi.org/10.1038/nature12060.

(5) Kraemer, M. U. G.; Reiner, R. C.; Brady, O. J.; Messina, J. P.; Gilbert, M.; Pigott, D. M.; Yi, D.; Johnson, K.; Earl, L.; Marczak, L. B.; Shirude, S.; Davis Weaver, N.; Bisanzio, D.; Perkins, T. A.; Lai, S.; Lu, X.; Jones, P.; Coelho, G. E.; Carvalho, R. G.; Van Bortel, W.; Marsboom, C.; Hendrickx, G.; Schaffner, F.; Moore, C. G.; Nax, H. H.; Bengtsson, L.; Wetter, E.; Tatem, A. J.; Brownstein, J. S.; Smith, D. L.; Lambrechts, L.; Cauchemez, S.; Linard, C.; Faria, N. R.; Pybus, O. G.; Scott, T. W.; Liu, Q.; Yu, H.; Wint, G. R. W.; Hay, S. I.; Golding, N. Past and Future Spread of the Arbovirus Vectors *Aedes Aegypti* and *Aedes Albopictus*. *Nat. Microbiol.* **2019**, *4* (5), 854–863. https://doi.org/10.1038/s41564-019-0376-y.

(6) Franklinos, L. H. V.; Jones, K. E.; Redding, D. W.; Abubakar, I. The Effect of Global Change on Mosquito-Borne Disease. *Lancet Infect. Dis.* **2019**, *19* (9), e302–e312. https://doi.org/10.1016/S1473-3099(19)30161-6.

(7) Samal, R. R.; Gupta, S.; Kumar, S. An Overview of Factors Affecting Dengue Transmission in Asian Region and Its Predictive Models. *J. Appl. Nat. Sci.* **2020**, *12* (3), 460–470. https://doi.org/10.31018/jans.v12i3.2360.

(8) Nakase, T.; Giovanetti, M.; Obolski, U.; Lourenço, J. Population at Risk of Dengue Virus Transmission Has Increased Due to Coupled Climate Factors and Population Growth. *Commun. Earth Environ.* **2024**, *5* (1), 1–11. https://doi.org/10.1038/s43247-024-01639-6.

(9) Kok, B. H.; Lim, H. T.; Lim, C. P.; Lai, N. S.; Leow, C. Y.; Leow, C. H. Dengue Virus Infection – a Review of Pathogenesis, Vaccines, Diagnosis and Therapy. *Virus Res.* **2023**, *324*, 199018. https://doi.org/10.1016/j.virusres.2022.199018.

(10) Battisti, V.; Urban, E.; Langer, T. Antivirals against the Chikungunya Virus. *Viruses* **2021**, *13* (7), 1307. https://doi.org/10.3390/v13071307.

(11) de Lima Cavalcanti, T. Y. V.; Pereira, M. R.; de Paula, S. O.; Franca, R. F. de O. A Review on Chikungunya Virus Epidemiology, Pathogenesis and Current Vaccine Development. *Viruses* **2022**, *14* (5), 969. https://doi.org/10.3390/v14050969.

(12) Dahiya, N.; Yadav, M.; Singh, H.; Jakhar, R.; Sehrawat, N. ZIKV: Epidemiology, Infection Mechanism and Current Therapeutics. *Front. Trop. Dis.* **2023**, *3*. https://doi.org/10.3389/fitd.2022.1059283.

(13) He, Y.; Zhou, J.; Gao, H.; Liu, C.; Zhan, P.; Liu, X. Broad-Spectrum Antiviral Strategy: Host-Targeting Antivirals against Emerging and Re-Emerging Viruses. *Eur. J. Med. Chem.* **2024**, *265*, 116069. https://doi.org/10.1016/j.ejmech.2023.116069.

(14) Neufeldt, C. J.; Cortese, M.; Acosta, E. G.; Bartenschlager, R. Rewiring Cellular Networks by Members of the Flaviviridae Family. *Nat. Rev. Microbiol.* **2018**, *16* (3), 125–142. https://doi.org/10.1038/nrmicro.2017.170.

(15) Chambon, M.; Herrscher, C.; Al Halabi, D.; François, N.; Belouzard, S.; Boutet, S.; Pham, V. C.; Doan, T. M. H.; Séron, K.; Mavingui, P.; Litaudon, M.; El Kalamouni, C.; Apel, C. New Phenolic Lipids from the Leaves of *Clausena Harmandiana* Inhibit SARS-CoV-2 Entry into Host Cells. *Molecules* **2023**, *28* (14), 5414. https://doi.org/10.3390/molecules28145414.

(16) Petit, B.; Marguerite, E.; Van Elslande, E.; Nedev, H.; Iorga, B. I.; Pham, V. C.; Doan, T. M. H.; Séron, K.; Litaudon, M.; El Kalamouni, C.; Apel, C. Antiviral Miliusanes and Isolation of an Unprecedented Miliusane Dimer from *Miliusa Balansae*. *Fitoterapia* **2024**, *177*, 106083. https://doi.org/10.1016/j.fitote.2024.106083.

(17) Olivon, F.; Allard, P.-M.; Koval, A.; Righi, D.; Genta-Jouve, G.; Neyts, J.; Apel, C.; Pannecouque, C.; Nothias, L.-F.; Cachet, X.; Marcourt, L.; Roussi, F.; Katanaev, V. L.; Touboul, D.; Wolfender, J.-L.; Litaudon, M. Bioactive Natural Products Prioritization Using Massive Multi-Informational Molecular Networks. *ACS Chem. Biol.* **2017**, *12* (10), 2644–2651. https://doi.org/10.1021/acschembio.7b00413.

(18) Olivon, F.; Remy, S.; Grelier, G.; Apel, C.; Eydoux, C.; Guillemot, J.-C.; Neyts, J.; Delang, L.; Touboul, D.; Roussi, F.; Litaudon, M. Antiviral Compounds from *Codiaeum Peltatum* Targeted by a Multi-Informative Molecular Networks Approach. *J. Nat. Prod.* **2019**, *82* (2), 330–340. https://doi.org/10.1021/acs.jnatprod.8b00800.

(19) Olivon, F.; Apel, C.; Retailleau, P.; Allard, P. M.; Wolfender, J. L.; Touboul, D.; Roussi, F.; Litaudon, M.; Desrat, S. Searching for Original Natural Products by Molecular Networking: Detection, Isolation and Total Synthesis of Chloroaustralasines. *Org. Chem. Front.* **2018**, *5* (14), 2171–2178. https://doi.org/10.1039/C8QO00429C.

(20) Olivon, F.; Retailleau, P.; Desrat, S.; Touboul, D.; Roussi, F.; Apel, C.; Litaudon, M. Isolation of Picrotoxanes from *Austrobuxus Carunculatus* Using Taxonomy-Based Molecular Networking. *J. Nat. Prod.* **2020**, *83* (10), 3069–3079. https://doi.org/10.1021/acs.jnatprod.0c00636.

(21) Hartley, T. G. A Revision of the Genus *Comptonella* (Rutaceae). *Bull. Muséum Natl. Hist. Nat. Sect. BAdansonia Bot. Phytochim.* **1983**, *5* (4), 391–413.

(22) Baudouin, G.; Tillequin, F.; Koch, M.; Pusset, J.; Sévenet, T. Plantes de Nouvelle-Calédonie. LXXIII. Alcaloïdes de *Dutaillyea Oreophila* et de *Dutaillyea Drupacea*. *J. Nat. Prod.* **1981**, *44* (5), 546–550. https://doi.org/10.1021/np50017a006.

(23) Pusset, J.; Lopez, J. L.; Pais, M.; Neirabeyeh, M. A.; Veillon, J.-M. Isolation and 2D NMR Studies of Alkaloids from *Comptonella Sessilifoliola*. *Planta Med.* **2007**, *57*, 153–155. https://doi.org/10.1055/s-2006-960053.

(24) Muyard, F.; Bevalot, F.; Laude, B.; Vaquette, J. Alkaloids from Stem Bark of *Dutaillyea Baudouinii*. *Phytochemistry* **1992**, *31* (3), 1087–1089. https://doi.org/10.1016/0031-9422(92)80090-2.

(25) Girard, C.; Muyard, F.; Bévalot, F.; Tillequin, F.; Vaquette, J.; Sévenet, T.; Litaudon, M. Polyoxygenated Flavones from the Leaves of *Comptonella Microcarpa*. *J. Nat. Prod.* **1999**, *62* (8), 1188–1189. https://doi.org/10.1021/np9900730.

(26) Gadea, G.; Bos, S.; Krejbich-Trotot, P.; Clain, E.; Viranaicken, W.; El-Kalamouni, C.; Mavingui, P.; Desprès, P. A Robust Method for the Rapid Generation of Recombinant Zika Virus Expressing the GFP Reporter Gene. *Virology* **2016**, *497*, 157–162. https://doi.org/10.1016/j.virol.2016.07.015.

(27) Appelhans, M. S.; Wen, J.; Wagner, W. L. A Molecular Phylogeny of *Acronychia*, *Euodia*, *Melicope* and Relatives (Rutaceae) Reveals Polyphyletic Genera and Key

Innovations for Species Richness. *Mol. Phylogenet. Evol.* **2014**, *79*, 54–68. https://doi.org/10.1016/j.ympev.2014.06.014.

(28) Schmid, R.; Heuckeroth, S.; Korf, A.; Smirnov, A.; Myers, O.; Dyrlund, T. S.; Bushuiev, R.; Murray, K. J.; Hoffmann, N.; Lu, M.; Sarvepalli, A.; Zhang, Z.; Fleischauer, M.; Dührkop, K.; Wesner, M.; Hoogstra, S. J.; Rudt, E.; Mokshyna, O.; Brungs, C.; Ponomarov, K.; Mutabdžija, L.; Damiani, T.; Pudney, C. J.; Earll, M.; Helmer, P. O.; Fallon, T. R.; Schulze, T.; Rivas-Ubach, A.; Bilbao, A.; Richter, H.; Nothias, L.-F.; Wang, M.; Orešič, M.; Weng, J.-K.; Böcker, S.; Jeibmann, A.; Hayen, H.; Karst, U.; Dorrestein, P. C.; Petras, D.; Du, X.; Pluskal, T. Integrative Analysis of Multimodal Mass Spectrometry Data in MZmine 3. *Nat. Biotechnol.* **2023**, *41* (4), 447–449. https://doi.org/10.1038/s41587-023-01690-2.

(29) Olivon, F.; Elie, N.; Grelier, G.; Roussi, F.; Litaudon, M.; Touboul, D. MetGem Software for the Generation of Molecular Networks Based on the T-SNE Algorithm. *Anal. Chem.* **2018**, *90* (23), 13900–13908. https://doi.org/10.1021/acs.analchem.8b03099.

(30) Dührkop, K.; Fleischauer, M.; Ludwig, M.; Aksenov, A. A.; Melnik, A. V.; Meusel, M.; Dorrestein, P. C.; Rousu, J.; Böcker, S. SIRIUS 4: A Rapid Tool for Turning Tandem Mass Spectra into Metabolite Structure Information. *Nat. Methods* **2019**, *16* (4), 299–302. https://doi.org/10.1038/s41592-019-0344-8.

(31) Shimokawa, K.; Mashima, I.; Asai, A.; Yamada, K.; Kita, M.; Uemura, D. (−)-Ternatin, a Highly N-Methylated Cyclic Heptapeptide That Inhibits Fat Accumulation: Structure and Synthesis. *Tetrahedron Lett.* **2006**, *47* (26), 4445–4448. https://doi.org/10.1016/j.tetlet.2006.04.073.

(32) Blunt, J.; Cole, T.; Munro, M.; Sun, L.; Weber, J.-F. R.; Ramasamy, K.; Bakar, H. A.; Majeed, A. B. B. A. Bioactive Compounds. WO2010062159A1, **2010**.

(33) Wang, H.-Y.; Yang, H.; Holm, M.; Tom, H.; Oltion, K.; Al-Khdhairawi, A. A. Q.; Weber, J.-F. F.; Blanchard, S. C.; Ruggero, D.; Taunton, J. Synthesis and Single-Molecule Imaging Reveal Stereospecific Enhancement of Binding Kinetics by the Antitumour eEF1A Antagonist SR-A3. *Nat. Chem.* **2022**, *14* (12), 1443–1450. https://doi.org/10.1038/s41557-022-01039-3.

(34) Carelli, J. D.; Sethofer, S. G.; Smith, G. A.; Miller, H. R.; Simard, J. L.; Merrick, W. C.; Jain, R. K.; Ross, N. T.; Taunton, J. Ternatin and Improved Synthetic Variants Kill Cancer Cells by Targeting the Elongation Factor-1A Ternary Complex. *eLife* **2015**, *4*, e10222. https://doi.org/10.7554/eLife.10222.

(35) Voronkino, T. M.; Koreneva, V. M.; Kursanova, G. V.; Muchak, E. T.; Onoprienko, V. V.; Kolossov, M. N. Russ. Pat. N517198.

(36) Feng, Y.; Blunt, J. W.; Cole, A. L. J.; Cannon, J. F.; Robinson, W. T.; Munro, M. H. G. Two Novel Cytotoxic Cyclodepsipeptides from a Mycoparasitic *Cladobotryum* Sp. *J. Org. Chem.* **2003**, *68* (5), 2002–2005. https://doi.org/10.1021/jo0263059.

(37) Jayasuriya, H.; Zink, D. L.; Polishook, J. D.; Bills, G. F.; Dombrowski, A. W.; Genilloud, O.; Pelaez, F. F.; Herranz, L.; Quamina, D.; Lingham, R. B.; Danzeizen, R.; Graham, P. L.; Tomassini, J. E.; Singh, S. B. Identification of Diverse Microbial Metabolites as Potent Inhibitors of HIV-1 Tat Transactivation. *Chem. Biodivers.* **2005**, *2* (1), 112–122. https://doi.org/10.1002/cbdv.200490162.

(38) Shimokawa, K.; Yamada, K.; Kita, M.; Uemura, D. Convergent Synthesis and in Vivo Inhibitory Effect on Fat Accumulation of (−)-Ternatin, a Highly N-Methylated Cyclic Peptide. *Bioorg. Med. Chem. Lett.* **2007**, *17* (16), 4447–4449. https://doi.org/10.1016/j.bmcl.2007.06.015.

(39) Shimokawa, K.; Iwase, Y.; Miwa, R.; Yamada, K.; Uemura, D. Whole Structure−Activity Relationships of the Fat-Accumulation Inhibitor (−)-Ternatin:

Recognition of the Importance of Each Amino Acid Residue. *J. Med. Chem.* **2008**, *51* (19), 5912–5914. https://doi.org/10.1021/jm800741n.

(40) Shimokawa, K.; Mashima, I.; Asai, A.; Ohno, T.; Yamada, K.; Kita, M.; Uemura, D. Biological Activity, Structural Features, and Synthetic Studies of (−)-Ternatin, a Potent Fat-Accumulation Inhibitor of 3T3-L1 Adipocytes. *Chem. – Asian J.* **2008**, *3* (2), 438–446. https://doi.org/10.1002/asia.200700243.

(41) Shimokawa, K.; Yamada, K.; Uemura, D. Structure-Based Hybridization of the Bioactive Natural Products Rhizonin A and Ternatin Leading to a Selective Fat-Accumulation Inhibitor against 3T3-L1 Adipocytes. *Bioorg. Med. Chem. Lett.* **2009**, *19* (3), 867–869. https://doi.org/10.1016/j.bmcl.2008.11.109.

(42) Shimokawa, K.; Miwa, R.; Yamada, K.; Uemura, D. Importance of the Backbone Conformation of (−)-Ternatin in Its Fat-Accumulation Inhibitory Activity against 3T3-L1 Adipocytes. *Org. Biomol. Chem.* **2009**, *7* (4), 777–784. https://doi.org/10.1039/B818903J.

(43) Ito, M.; Ito, J.; Kitazawa, H.; Shimamura, K.; Fukami, T.; Tokita, S.; Shimokawa, K.; Yamada, K.; Kanatani, A.; Uemura, D. (−)-Ternatin Inhibits Adipogenesis and Lipid Metabolism in 3T3-L1 Cells. *Peptides* **2009**, *30* (6), 1074–1081. https://doi.org/10.1016/j.peptides.2009.02.008.

(44) Kobayashi, M.; Kawashima, H.; Takemori, K.; Ito, H.; Murai, A.; Masuda, S.; Yamada, K.; Uemura, D.; Horio, F. Ternatin, a Cyclic Peptide Isolated from Mushroom, and Its Derivative Suppress Hyperglycemia and Hepatic Fatty Acid Synthesis in Spontaneously Diabetic KK-*Ay* Mice. *Biochem. Biophys. Res. Commun.* **2012**, *427* (2), 299–304. https://doi.org/10.1016/j.bbrc.2012.09.045.

(45) Kawazoe, Y.; Tanaka, Y.; Omura, S.; Uemura, D. Design, Synthesis, and Evaluation, Derivatives of the Fat-Accumulation Inhibitor Ternatin: Toward Ternatin Molecular

Probes. *Tetrahedron Lett.* **2014**, *55* (32), 4445–4447. https://doi.org/10.1016/j.tetlet.2014.06.036.

(46) Gordon, D. E.; Jang, G. M.; Bouhaddou, M.; Xu, J.; Obernier, K.; White, K. M.; O'Meara, M. J.; Rezelj, V. V.; Guo, J. Z.; Swaney, D. L.; Tummino, T. A.; Hüttenhain, R.; Kaake, R. M.; Richards, A. L.; Tutuncuoglu, B.; Foussard, H.; Batra, J.; Haas, K.; Modak, M.; Kim, M.; Haas, P.; Polacco, B. J.; Braberg, H.; Fabius, J. M.; Eckhardt, M.; Soucheray, M.; Bennett, M. J.; Cakir, M.; McGregor, M. J.; Li, Q.; Meyer, B.; Roesch, F.; Vallet, T.; Mac Kain, A.; Miorin, L.; Moreno, E.; Naing, Z. Z. C.; Zhou, Y.; Peng, S.; Shi, Y.; Zhang, Z.; Shen, W.; Kirby, I. T.; Melnyk, J. E.; Chorba, J. S.; Lou, K.; Dai, S. A.; Barrio-Hernandez, I.; Memon, D.; Hernandez-Armenta, C.; Lyu, J.; Mathy, C. J. P.; Perica, T.; Pilla, K. B.; Ganesan, S. J.; Saltzberg, D. J.; Rakesh, R.; Liu, X.; Rosenthal, S. B.; Calviello, L.; Venkataramanan, S.; Liboy-Lugo, J.; Lin, Y.; Huang, X.-P.; Liu, Y.; Wankowicz, S. A.; Bohn, M.; Safari, M.; Ugur, F. S.; Koh, C.; Savar, N. S.; Tran, Q. D.; Shengjuler, D.; Fletcher, S. J.; O'Neal, M. C.; Cai, Y.; Chang, J. C. J.; Broadhurst, D. J.; Klippsten, S.; Sharp, P. P.; Wenzell, N. A.; Kuzuoglu-Ozturk, D.; Wang, H.-Y.; Trenker, R.; Young, J. M.; Cavero, D. A.; Hiatt, J.; Roth, T. L.; Rathore, U.; Subramanian, A.; Noack, J.; Hubert, M.; Stroud, R. M.; Frankel, A. D.; Rosenberg, O. S.; Verba, K. A.; Agard, D. A.; Ott, M.; Emerman, M.; Jura, N.; von Zastrow, M.; Verdin, E.; Ashworth, A.; Schwartz, O.; d'Enfert, C.; Mukherjee, S.; Jacobson, M.; Malik, H. S.; Fujimori, D. G.; Ideker, T.; Craik, C. S.; Floor, S. N.; Fraser, J. S.; Gross, J. D.; Sali, A.; Roth, B. L.; Ruggero, D.; Taunton, J.; Kortemme, T.; Beltrao, P.; Vignuzzi, M.; García-Sastre, A.; Shokat, K. M.; Shoichet, B. K.; Krogan, N. J. A SARS-CoV-2 Protein Interaction Map Reveals Targets for Drug Repurposing. *Nature* **2020**, *583* (7816), 459–468. https://doi.org/10.1038/s41586-020-2286-9.

(47) White, K. M.; Rosales, R.; Yildiz, S.; Kehrer, T.; Miorin, L.; Moreno, E.; Jangra, S.; Uccellini, M. B.; Rathnasinghe, R.; Coughlan, L.; Martinez-Romero, C.; Batra, J.; Rojc, A.; Bouhaddou, M.; Fabius, J. M.; Obernier, K.; Dejosez, M.; Guillén, M. J.; Losada, A.; Avilés, P.; Schotsaert, M.; Zwaka, T.; Vignuzzi, M.; Shokat, K. M.; Krogan, N. J.; García-Sastre, A. Plitidepsin Has Potent Preclinical Efficacy against SARS-CoV-2 by Targeting the Host Protein eEF1A. *Science* **2021**, *371* (6532), 926–931. https://doi.org/10.1126/science.abf4058.

(48) Molina Molina, E.; Bech-Serra, J. J.; Franco-Trepat, E.; Jarne, I.; Perez-Zsolt, D.; Badia, R.; Riveira-Muñoz, E.; Garcia-Vidal, E.; Revilla, L.; Franco, S.; Tarrés-Freixas, F.; Roca, N.; Ceada, G.; Kochanowski, K.; Raïch-Regué, D.; Erkizia, I.; Boreika, R.; Bordoy, A. E.; Soler, L.; Guil, S.; Carrillo, J.; Blanco, J.; Martínez, M. Á.; Paredes, R.; Losada, A.; Aviles, P.; Cuevas, C.; Vergara-Alert, J.; Segalés, J.; Clotet, B.; Ballana, E.; de la Torre, C.; Izquierdo-Useros, N. Targeting eEF1A Reprograms Translation and Uncovers Broad-Spectrum Antivirals against Cap or m6A Protein Synthesis Routes. *Nat. Commun.* **2025**, *16* (1), 1087. https://doi.org/10.1038/s41467-025-56151-y.

(49) Breaud, C.; Lallemand, L.; Mares, G.; Mabrouki, F.; Bertolotti, M.; Simmler, C.; Greff, S.; Mauduit, M.; Herbette, G.; Garayev, E.; Lavergne, C.; Cesari, M.; Bun-Llopet, S.-S.; Baghdikian, B.; Garayev, E. LC-MS Based Phytochemical Profiling towards the Identification of Antioxidant Markers in Some Endemic Aloe Species from Mascarene Islands. *Antioxidants* **2023**, *12* (1), 50. https://doi.org/10.3390/antiox12010050.

(50) Myers, O. D.; Sumner, S. J.; Li, S.; Barnes, S.; Du, X. One Step Forward for Reducing False Positive and False Negative Compound Identifications from Mass Spectrometry Metabolomics Data: New Algorithms for Constructing Extracted Ion Chromatograms and Detecting Chromatographic Peaks. *Anal. Chem.* **2017**, *89* (17), 8696–8703. https://doi.org/10.1021/acs.analchem.7b00947.

(51) Schmid, R.; Petras, D.; Nothias, L.-F.; Wang, M.; Aron, A. T.; Jagels, A.; Tsugawa, H.; Rainer, J.; Garcia-Aloy, M.; Dührkop, K.; Korf, A.; Pluskal, T.; Kameník, Z.; Jarmusch, A. K.; Caraballo-Rodríguez, A. M.; Weldon, K. C.; Nothias-Esposito, M.; Aksenov, A. A.; Bauermeister, A.; Albarracin Orio, A.; Grundmann, C. O.; Vargas, F.; Koester, I.; Gauglitz, J. M.; Gentry, E. C.; Hövelmann, Y.; Kalinina, S. A.; Pendergraft, M. A.; Panitchpakdi, M.; Tehan, R.; Le Gouellec, A.; Aleti, G.; Mannochio Russo, H.; Arndt, B.; Hübner, F.; Hayen, H.; Zhi, H.; Raffatellu, M.; Prather, K. A.; Aluwihare, L. I.; Böcker, S.; McPhail, K. L.; Humpf, H.-U.; Karst, U.; Dorrestein, P. C. Ion Identity Molecular Networking for Mass Spectrometry-Based Metabolomics in the GNPS Environment. *Nat. Commun.* **2021**, *12* (1), 3832. https://doi.org/10.1038/s41467-021-23953-9.

(52) Shannon, P.; Markiel, A.; Ozier, O.; Baliga, N. S.; Wang, J. T.; Ramage, D.; Amin, N.; Schwikowski, B.; Ideker, T. Cytoscape: A Software Environment for Integrated Models of Biomolecular Interaction Networks. *Genome Res.* **2003**, *13* (11), 2498–2504. https://doi.org/10.1101/gr.1239303.

(53) Böcker, S.; Dührkop, K. Fragmentation Trees Reloaded. *J. Cheminformatics* **2016**, *8* (1), 5. https://doi.org/10.1186/s13321-016-0116-8.

(54) Böcker, S.; Letzel, M. C.; Lipták, Z.; Pervukhin, A. SIRIUS: Decomposing Isotope Patterns for Metabolite Identification†. *Bioinformatics* **2009**, *25* (2), 218–224. https://doi.org/10.1093/bioinformatics/btn603.

(55) Dührkop, K.; Nothias, L.-F.; Fleischauer, M.; Reher, R.; Ludwig, M.; Hoffmann, M. A.; Petras, D.; Gerwick, W. H.; Rousu, J.; Dorrestein, P. C.; Böcker, S. Systematic Classification of Unknown Metabolites Using High-Resolution Fragmentation Mass Spectra. *Nat. Biotechnol.* **2021**, *39* (4), 462–471. https://doi.org/10.1038/s41587-020-0740-8.

(56) Djoumbou Feunang, Y.; Eisner, R.; Knox, C.; Chepelev, L.; Hastings, J.; Owen, G.; Fahy, E.; Steinbeck, C.; Subramanian, S.; Bolton, E.; Greiner, R.; Wishart, D. S. ClassyFire: Automated Chemical Classification with a Comprehensive, Computable Taxonomy. *J. Cheminformatics* **2016**, *8* (1), 61. https://doi.org/10.1186/s13321-016-0174-y.

(57) Dührkop, K.; Shen, H.; Meusel, M.; Rousu, J.; Böcker, S. Searching Molecular Structure Databases with Tandem Mass Spectra Using CSI:FingerID. *Proc. Natl. Acad. Sci.* **2015**, *112* (41), 12580–12585. https://doi.org/10.1073/pnas.1509788112.

(58) Kim, H. W.; Wang, M.; Leber, C. A.; Nothias, L.-F.; Reher, R.; Kang, K. B.; van der Hooft, J. J. J.; Dorrestein, P. C.; Gerwick, W. H.; Cottrell, G. W. NPClassifier: A Deep Neural Network-Based Structural Classification Tool for Natural Products. *J. Nat. Prod.* **2021**, *84* (11), 2795–2807. https://doi.org/10.1021/acs.jnatprod.1c00399.

(59) Krejbich-Trotot, P.; Belarbi, E.; Ralambondrainy, M.; El-Kalamouni, C.; Viranaicken, W.; Roques, P.; Desprès, P.; Gadea, G. The Growth of Arthralgic Ross River Virus Is Restricted in Human Monocytic Cells. *Virus Res.* **2016**, *225*, 64–68. https://doi.org/10.1016/j.virusres.2016.09.007.

(60) Wilkinson, D. A.; Mercier, A.; Turpin, M.; Simbi, M.-A.; Turpin, J.; Lebarbenchon, C.; Cesari, M.; Jaffar-Bandjee, M.-C.; Josset, L.; Yemadje-Menudier, L.; Lina, B.; Mavingui, P. Genomic Evolution of SARS-CoV-2 in Reunion Island. *Infect. Genet. Evol.* **2022**, *106*, 105381. https://doi.org/10.1016/j.meegid.2022.105381.